

A Thesis

entitled

Exploring RayStation Treatment Planning System: Commissioning Varian TrueBeam
Photon and Electron Energies, and Feasibility of Using FFF Photon Beam to Deliver
Conventional Flat Beam

by

Jui Wan

Submitted to the Graduate Faculty as partial fulfillment of the requirements for the
Master of Science Degree in Biomedical Science: Medical Physics

Dr. E. Ishmael Parsai, Committee Chair

Dr. Diana Shvydka, Committee Member

Dr. Nicholas Sperling, Committee Member

Dr. Amanda Bryant-Friedrich, Dean
College of Graduate Studies

The University of Toledo

August 2017

Copyright 2017, Jui Wan

This document is copyrighted material. Under copyright law, no parts of this document may be reproduced without the expressed permission of the author.

An Abstract of

Exploring RayStation Treatment Planning System: Commissioning Varian TrueBeam Photon and Electron Energies, and Feasibility of Using FFF Photon Beam to Deliver Conventional Flat Beam

by

Jui Wan

Submitted to the Graduate Faculty as partial fulfillment of the requirements for the Master of Science Degree in Biomedical Science: Medical Physics

The University of Toledo

August 2017

RayStation, a new treatment planning system (TPS), was purchased and recently commissioned for clinical use by the institution. As part of the commissioning process, an accurate model of the TrueBeam linear accelerator was made prior to clinical acceptances. Data collection, importing measurements, beam modeling, point dose verifications and clinical plan comparisons are procedures that must be done in order to complete the commissioning of photon and electron energies. During the beam modeling process, various parameters were modified to achieve close matches between the computed and measured PDD curves, as well as measured and computed beam profiles. The tolerance objectives were to have computed data deviating from the measured data within the 2% in fall-off regions, 3% tolerance within in-field and out-of-field regions, and 10% tolerance in build-up regions and penumbra regions ^[1]. The dosimetric validation procedure followed. Point dose measurements were completed using both the ArcCHECK phantom and the water tank. The majority of the results met the set criteria except for some measurements blocked by MLC leaves or jaws when taken adjacent to the edge of fields. To further confirm the goodness of modeled beams, clinical treatment

plans developed with the previously clinically commissioned Pinnacle TPS and imported into the RayStation TPS to generate new plans with same beam arrangements and control points and used as comparisons.

After clinical commissioning was completed for RayStation software, a feasibility of using FFF beams to deliver identical or superior beam profile provided by conventional flattened beams of the same energy was investigated. The objective of this research was to show that through sliding window treatment planning, one can create optimized plans and hence no longer the technology of flattening filter is required in modern linear accelerators. To explore this topic, a two stage analysis was carried out. First, delivering doses in a water cube with 10×10 to 30×30 cm² open-field 6 MV flattened beams and also create 0.1cm thick square plane structures to be used when undergo the optimization process with 6 FFF beams. Then scaling doses to prescribe 100 cGy at the center of the plane for comparison purpose. The overall uniformity of line profile for FFF beams across the CAX at 10 cm depth showed 1% to 2% superior to flattened beams.

For the clinical treatment plans comparison, ten patients were selected with five head and neck cancer plans as well as five lung and mediastinum cancer plans. Original plans were all completed with 6 MV flattened beams and approved by radiation oncologists. New plans were accomplished with 6 FFF beams and same coverages of PTVs were achieved. Most of average mean doses to critical structures and normal tissue volumes receiving 5%, 10%, 20% and 30% of the prescription dose were reduced with FFF plans with slightly increased average max doses.

To all of my family members for always supporting and encouraging me.

Acknowledgements

First of all, I wish to express my appreciation of Dr. Parsai for guiding me in precise directions to the final goal of this research, and also for spurring me on to have more confidences every time frustrations were encountered. Second, I would like to thank Dr. Sperling for offering all of his knowledge regarding the photon beam modeling, and Dr. Shvydka and Dr. Pearson for sharing educational materials and their experience leading me down the correct path to become a professional medical physicist. Moreover, I also want to express my thanks to Noah Staley for teaching me about work in the clinic and helping me finish this thesis successfully.

Table of Contents

Abstract	iii
Acknowledgements	v
Table of Contents	vi
List of Tables	ix
List of Figures	x
List of Abbreviations	xii
1 Chapter 1: Introduction	1
1.1 Treatment planning system RayStation	1
1.1.1 Dose engines	1
1.2 Linear accelerator TrueBeam model.....	2
1.2.1 Photon source.....	4
1.2.2 Electron source.....	5
1.3 Commissioning the new treatment planning system	5
1.4 Beam qualities.....	6
1.4.1 Flat beam.....	7
1.4.2 FFF beam	7
1.5 Intensity-modulated radiation therapy (IMRT)	7
2 Chapter 2: Methods and materials for commissioning the RayStation TPS.....	9
2.1 Data collection for photons.....	9

	2.2 Data collection for electrons	11
	2.2.1 Air profiles	12
	2.2.2 Open water depth dose.....	13
	2.2.3 Water depth dose with applicators	13
	2.3 Equipment used for measurements	15
	2.4 Beam modeling	16
	2.4.1 Photon beams modeling.....	16
	2.4.1.1 Auto-modeling	16
	2.4.1.2 Manual beam modeling.....	19
	2.4.1.3 FFF beam modeling	24
	2.4.2 Electron beams modeling.....	24
	2.5 Point dose measurements for verification.....	30
	2.5.1 Measurements in homogeneous and inhomogeneous media	30
	2.5.2 Point dose measurements in the water tank	32
	2.6 Treatment plans comparison for validation	33
3	Chapter 3: Methods and materials for the feasibility of using FFF beams to deliver conventional flat beams	34
	3.1 General concepts of using FFF beams to deliver flat beams	34
	3.1.1 Methods and materials	35
	3.2 Main purposes for clinical treatment plans comparison	36
	3.2.1 Methods and materials	36
4	Chapter 4: Results and discussions for commissioning the RayStation TPS	39

4.1	Beam modeling results.....	39
4.1.1	Photons.....	40
4.1.2	Electrons	44
4.2	Point dose measurements in homogeneous and inhomogeneous media.....	50
4.3	Point dose measurements in a water tank	51
4.4	Treatment plans comparison for validation	52
4.5	Discussions	55
4.5.1	Beam modeling	55
4.5.2	Dosimetric validation.....	55
5	Chapter 5: Results and discussions for the feasibility of using FFF beam to deliver conventional flat beam.....	57
5.1	Utilizing flat dose distributions by FFF beams.....	57
5.1.1	Discussions	60
5.2	Clinical treatment plans comparison.....	60
5.2.1	Discussions	62
6	Chapter 6: Conclusions	63
	References.....	65
A	Summary of adjustable beam modeling parameters	66
B	Results of point dose measurements in the water tank for commissioning	71
C	Clinical treatment plans comparison.....	75

List of Tables

2-1	Minimum depths for measuring the bremsstrahlung tail	14
2-2	Shallow depths (high dose region) for beam profile measurement with different energy ranges.	15
2-3	Detectors utilized for commissioning data	15
3-1	Dose levels for individual head and neck cancer patient	37
3-2	Dose levels for individual lung/mediastinum cancer patient	37
4-1	Analysis of average fit qualities and standard deviations for PDDs and profiles..	43
4-2	Analysis of fit qualities for PDDs and profiles	48
4-3	Results from both actual measurements and RayStation TPS	50
5-1	Percentage uniformities for flat beams and FFF beams.....	59
A-1	Beam parameters for photons	66
A-2	Beam parameters for electrons.....	68
B-1	Measured point doses in the water tank	71
B-2	Computed point doses in the RayStation TPS	72
B-3	Percentage point dose differences between measured data and computed data	73

List of Figures

1-1	Overview of a LINAC machine	3
1-2	Detailed configuration of the Varian LINAC head for photons	4
2-1	The coordinate system of the linear accelerator	10
2-2	Open air profile measurements at 75 cm and 95 cm SDD.....	13
2-3	The operating window for the auto-modeling process	17
2-4	Energy spectrum for a regular 6 MV beam	18
2-5	The 6 MV $10 \times 10 \text{ cm}^2$ field size PDD curve changes after increasing the fluence for the 1 MV energy bin.....	20
2-6	The 6 MV $10 \times 10 \text{ cm}^2$ field size PDD curve changes after increasing both C and E0 for getting more precise fit within the build-up region	21
2-7	Decreasing weights of the flattening filter source	22
2-8	Declining the penumbra by decreasing the width of the primary source for a 6 MV beam with $10 \times 10 \text{ cm}^2$ field size at all depths.....	23
2-9	Decreasing the transmissions through the x jaw.....	24
2-10	Example of parameters for describing the electron energy spectrum for energy of 20 MeV	25
2-11	Electron energy spectrum for 20 MeV with parameters in the figure 2-10.....	26
2-12	Increasing delta E to raise the shoulder portion and decreasing E0 to shift the fall-off portion to a shallower depth.....	27

2-13	Parameters capable of modifying the 20 MeV electron beam profile	28
2-14	Functions of individual parameter for electron beam profile modification	29
2-15	Beam arrangement and dose distribution in RayStation.....	32
2-16	The irregular field (L-shape)	33
4-1	Final photons' computed and measured PDD curves with all FS and cross-plane beam profiles for each energy at all depths	43
4-2	Final electrons' computed and measured PDD curves and in-plane beam profiles for each energy, with applicators respectively.....	48
4-3	DVHs comparison for different plans.....	54
5-1	Axial views of the dose distribution for the 6 FFF beam as well as the 6 MV flat beam in a water cube.....	58
5-2	Differences of average maximum doses, mean doses and volumes receiving 5%, 10%, 20% and 30% of the prescription dose between 6 MV and 6 FFF.....	61
A-1	Electron source phase space parameters	69
C-1	Example of the sagittal-view dose distribution in a head and neck cancer treatment plans	75
C-2	Example of the coronal-view dose distribution in a lung and mediastinum cancer treatment plans	76

List of Abbreviations

TERMA.....	Total Energy Released per unit Mass
CC	Collapsed Cone algorithm
LINAC	Linear Accelerator
MLC.....	Multi-Leaf Collimator
FFF.....	Flattening-Filter Free
MV	Mega Voltage
MeV	Mega Electron Voltage
DICOM	Digital Imaging Communications in Medicine
STD	Standard Deviation
TPS.....	Treatment Planning System
DVH.....	Dose-Volume Histogram
PDD.....	Percent Depth Dose
d_m	Depth with the maximum dose
AP	Anterior-posterior
SSD	Source to Surface Distance
SAD	Source to Axis Distance
SDD.....	Source to Detector Distance
FS	Field Size
RMS	Root Mean Square
PMMA	Polymethyl Methacrylate
CT	Computed Tomography
MU	Monitor Unit
fx	Fractionation
CAX	Central Axis
IMRT.....	Intensity-Modulated Radiation Therapy
VMAT.....	Volumetric Modulated Arc Therapy
PTV	Planning Target Volume
cGy.....	centi-Gray
AAPM.....	the American Association of Physicists in Medicine
MAX	Maximum

Chapter 1

Introduction

1.1 Treatment planning system RayStation

In our institution, the department of Radiation oncology purchased a new treatment planning system (TPS) named RayStation, which was designed and sold by RaySearch Corporation. RayStation is powerful software for generating clinical treatment plans and offering numerous tools to analyze and optimize plans prior to implementing for patient radiation therapy treatment. It contains numerous adjustable set-up parameters to create different beam configurations and techniques, which can be used to deliver conformal dose distributions to delineated targets while reducing the radiation exposure to the surrounding normal tissues.

1.1.1 Dose engines

In the RayStation TPS, the computational dose engine for photon beams is Collapsed Cone (CC) algorithm, and electron dose is calculated by Monte Carlo simulation.

To put it briefly, the CC dose algorithm calculates dose in three steps: the energy fluence computation, the TERMA computation, and the point-spread kernel convolution.

The photon fluence is calculated based on a multi-source model: the primary source shapes the target and the secondary source shapes the flattening filter. Both sources are modeled with Gaussian profiles. The primary source has an elliptical intensity profile, while the secondary source has a circular intensity profile. The point-spread kernels used in the algorithm were pre-calculated with a Monte Carlo system developed for high energy physics simulations ^[2]. TERMA is computed in individual voxels based on the radiological depth, the mass density, the linear attenuation coefficient, and the energy fluence. The dose is calculated from a point tracing out in different angular directions. At the voxel level, contributions from one of the intersected voxels is computed by adding up kernels along the radiological length and scaling it with the intersected TERMA voxel.

The Monte Carlo algorithm uses the same method as the CC dose algorithm to compute energy fluence, and the dose calculation is based on a VMC++ algorithm in 3D voxel geometries.

1.2 Linear accelerator TrueBeam model

The TrueBeam linear accelerator at the University of Toledo Health Science Campus Dana Cancer Center was first used clinically in 2013. Primary components found in the linear accelerator are listed in the table below along with their particular functions and properties:

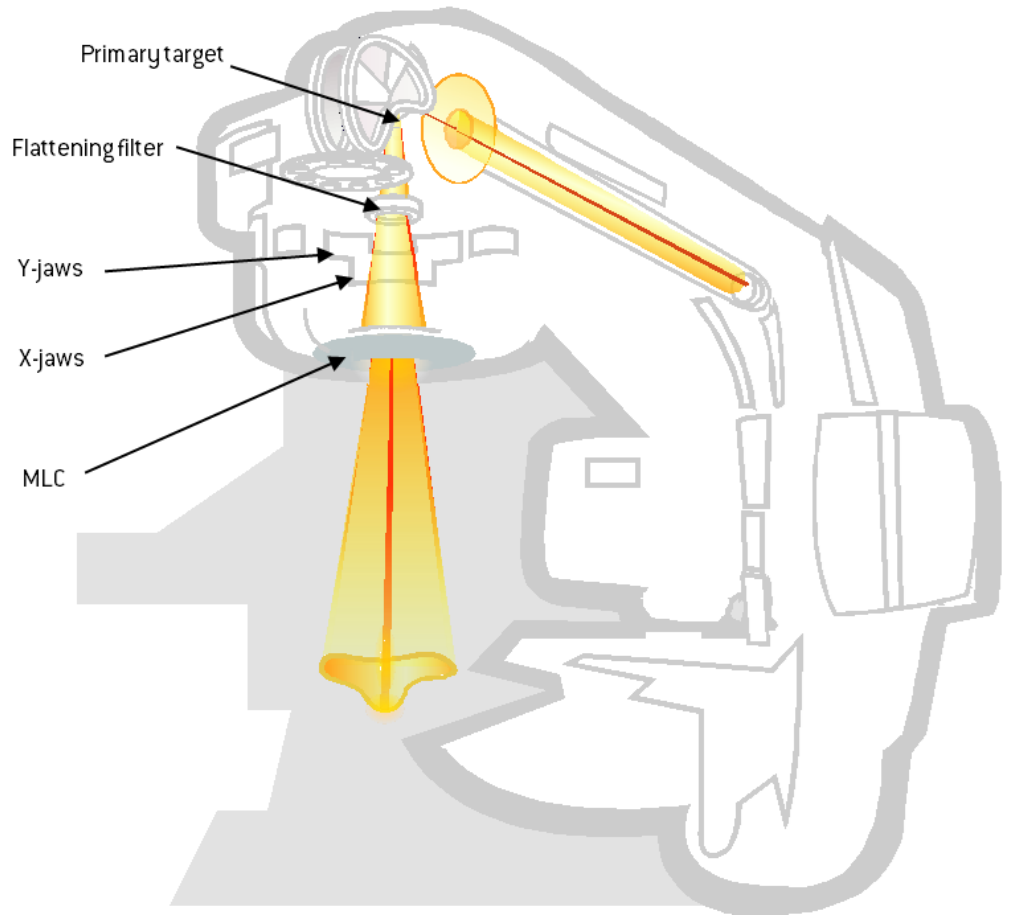


Figure 1-1: Overview of a LINAC machine (RayStation 5 RayPhysics Manual)

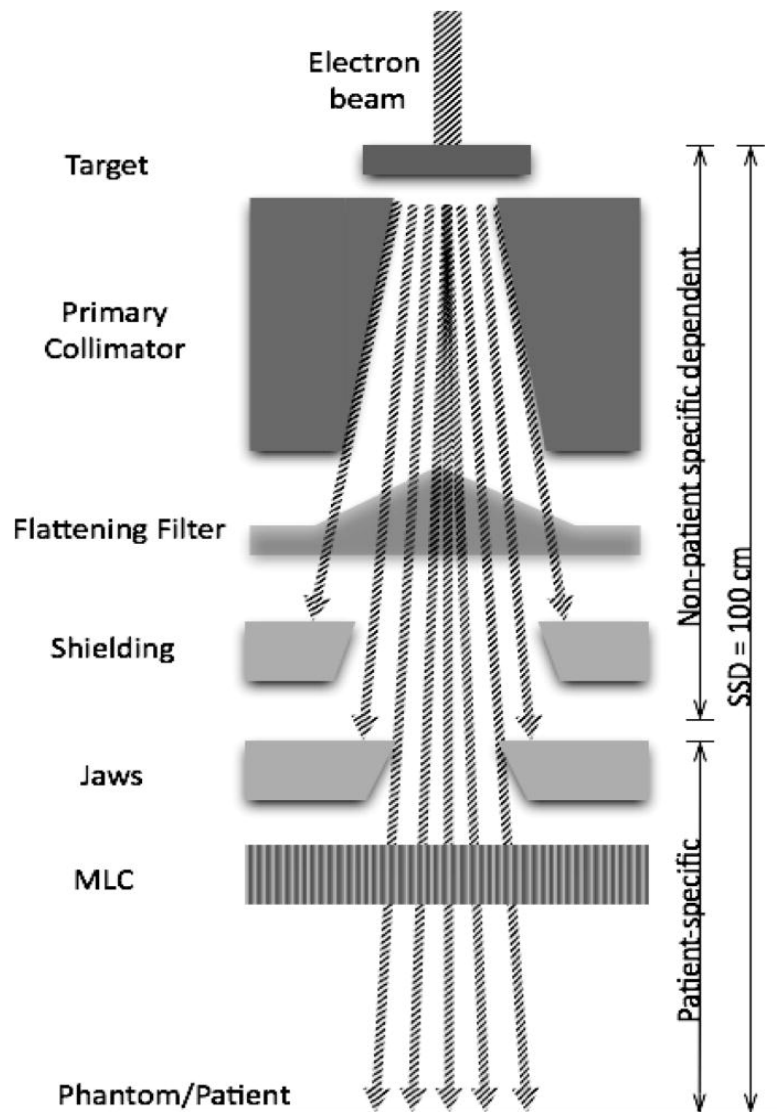


Figure 1-2: Detailed configuration of the Varian LINAC head for photons (Cecilia et. al ^[31])

1.2.1 Photon source

Three flattened beam energies (6 MV, 10 MV, and 18 MV) and a 6MV FFF energy were installed in the treatment machine head. During the production of a conventional flattened beam of radiation, accelerated electrons strike the target and produce photons, while the primary jaws are responsible to define the field size at a given distance from the target. The beam then passes through a cone shaped metal absorber (the

flattening filter) to absorb the more forward peaked photons at the beam center in contrast to those in the periphery to create a flat beam profile along both the cross-plane and in-plane directions. Before reaching the patient, secondary jaws and MLC leaves have the ability to define the patient specific field size and irregular field shape.

1.2.2 Electron source

Electron energies of 6 MeV, 9 MeV, 12 MeV, 16 MeV and 20 MeV were installed in the accelerator head. The production of electron beams requires the removal of the target, and the replacement of the flattening filter with the scattering foil, which is capable of expanding source of electrons to the useful size for radiation therapy.

1.3 Commissioning the new treatment planning system RayStation

Since the treatment planning software is new, it is important to make sure the system can be utilized with specific linear accelerators in clinic. Individual machines have distinct features and different outputs, and it is impossible to produce a treatment plan by a default beam configuration for every linear accelerator. The definitive characteristics of a linear accelerator measured, such as the percent depth dose and the beam profiles for different field sizes and energies, must be identical to what is modeled in the TPS, and the commissioning process is designed to fulfill these goals.

There are several steps that should be taken during the commissioning procedure, including measured data collection, importing measured data, modelling beam data, to achieve acceptable agreement between measured and modeled beams, point dose verifications in a phantom as well as a water tank, and as an added step, confirm dosimetric agreement between a formerly accepted treatment planning system and the

new one. The beam modelling and the verification sections will be emphasized because they directly relate to the research discussed later in this thesis.

1.4 Beam qualities

Photons and electrons of different energies travel different distances in medium, allowing for the treatment of tumors at various depths. In case of photon beams, the energy is specified in terms of nominal accelerator potential/ beam energy (MV or MeV), as well as in terms of a parameter which indicates penetrative quality of the beam. Commonly quoted penetrative quality indicator of the X-ray beam by the manufacturer is percentage depth dose at 10-cm depth (D_{10}) for $10 \times 10 \text{ cm}^2$ field size at the phantom surface and 100-cm source surface distance (SSD). For example typical published data for D_{10} for a generic 10-MV X-ray beam is $74.0 \pm 1.0\%$. In addition, the manufacturer also quotes the depth of dose maximum (d_m) as an alternative quality indicator of the beam. These two X-ray penetrative quality indicators suffer from the effect of electron contamination and may change their magnitude due to variation in components and accessories in the head of the accelerator. AAPM has adopted D_{10} as a quality-specifying parameter for X-rays under the recommendation that measurement should be done using 0.1-cm lead filter to limit the contribution of contamination electrons. Other recommended X-ray beam quality indicators are depth of 80% dose (d_{80}) for $10 \times 10 \text{ cm}^2$ field at an SSD of 100 cm along the central axis of the beam and the ratio of tissue phantom ratio (TPR) at the depths of 20 and 10 cm ($TPR_{20,10}$). For electrons, the beam quality is defined either as a Most Probable Energy, or Mean Energy. The most probable

energy is measured at the phantom surface as a function of R_p , the practical electron range, and the mean energy is defined as a function of R_{50} .

1.4.1 Flat beam

This type of beam is produced from a medical linear accelerator where a flattening filter has been introduced in the treatment head resulting in beam profiles with specific flatness and symmetry characteristics. This type of beam is often being used to deliver a uniform dose distribution. The flattening filter composed of high Z material and usually has a bell-shape. The beam uniformity is typically specified in terms of either transverse beam profiles or the uniformity index. For the case in which transverse beam profiles are used, the flatness and symmetry of the beam are specified over the central 80% of the beam profile at a depth of 10 cm in a water phantom for the largest field size of 40cm x 40 cm.

1.4.2 FFF beam

For flattening-filter free beams, the flattening filter in the treatment head is removed from the beam's path. Without the attenuation caused by the flattening filter, due to the diverging shape of the original beam, the intensity of photons along the central axis path will be the highest, reducing gradually as the edge of the beam field is approached. This type of beam is also symmetric and is usually being utilized for delivering extremely high doses at the center of tumors. This results in sharp dose fall-off at the edge of the field which spares adjacent normal structures.

1.5 Intensity-modulated radiation therapy (IMRT)

This technique has been introduced and applied to the clinic for a long period. Moving MLCs are used during the dose delivery, which is able to modulate the intensity of the beam to escalating higher doses deposited in the tumor and declining doses to adjacent normal structures. There are two categories of IMRT: step-and-shoot IMRT and sliding window IMRT.

For the step-and-shoot IMRT, radiation delivery and MLCs' movement happen separately, meaning radiation will be turned on right after MLCs already shifted to the expected location, and turned off while MLCs are moving. On the contrary, when dose delivery and MLCs' movement occur simultaneously, it will result in sliding window IMRT delivery when the radiation is on while MLCs are moving around.

Mechanism of optimizing IMRT treatment plans is using the inverse planning method, several objectives and constraints are established, such as the maximum dose, the minimum dose, the uniform dose and DVHs; then the treatment planning software will make effort to generate a plan to satisfy those objectives and constraints.

Chapter 2

Methods and materials for commissioning the RayStation TPS

2.1 Data collection for photons

All data was measured in a water tank, including depth dose curves on the central axis, beam profiles in x and y directions, output factors, and the absolute dose calibration point for reference field sizes. Before conducting any measurements, understanding of the coordinate system of the accelerator is necessary to ensure the acquired data is correct when the time comes to import it into the treatment planning system. The following figure displays the coordinate system of the linear accelerator.

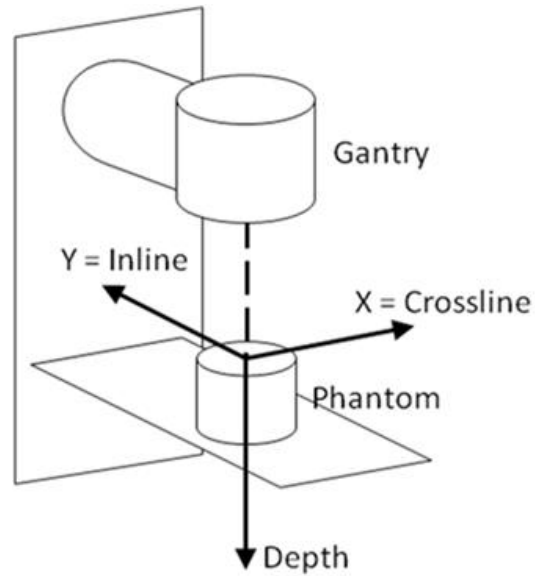


Figure 2-1: The coordinate system of the linear accelerator

Depth dose curves for every specified field size, with corresponding beam profiles were measured ($3 \times 3 \text{ cm}^2$, $5 \times 5 \text{ cm}^2$, $7 \times 7 \text{ cm}^2$, $10 \times 10 \text{ cm}^2$, $15 \times 15 \text{ cm}^2$, $20 \times 20 \text{ cm}^2$, $25 \times 25 \text{ cm}^2$, $30 \times 30 \text{ cm}^2$, $35 \times 35 \text{ cm}^2$, and $40 \times 40 \text{ cm}^2$). The $10 \times 10 \text{ cm}^2$ field size is required to be used as the reference field; all other field sizes are optional. These other field sizes were chosen to represent the range of related field sizes that are used for clinical treatment planning. Additionally, beam profiles at the depth of maximum dose (individually, it is 1.5 cm for 6 FFF, 1.6 cm for 6 MV, 2.4 cm for 10 MV and 3.3 cm for 18 MV), for 5 cm, 10 cm, 15 cm, and 20 cm fields were obtained with the water tank. Although RayStation does not require both inline and crossline profiles, two directions of the beam profile were measured to construct a more complete model. To summarize, depth dose curves and beam profiles should be obtained while considering the following:

1. Output factors for every field size, measured along the central axis. This factor should be normalized using the $10 \times 10 \text{ cm}^2$ reference field.
2. Depth at which output factors were measured. It is 10 cm for all photon energies, including 6MV FFF, 6MV, 10MV and 18MV.
3. The height and width of the detectors that were being used for measurements so the active volume of the detector can be determined. Most important of all, the relevant height and width corresponding to the orientation of the detectors that were used during the measuring process.
4. Detailed descriptions of the positions of the jaws and MLC leaves that define field size individually or simultaneously. It is the responsibility of the physicist to confirm all data was measured with field sizes shaped with identical methods for all energies.

Some other parameters must also be fixed for all measurements, including the SSD (source to surface distance) set at 100 cm, the gantry and collimator angles set to be 0 degrees, and the phantom size, which should be the same as the water tank placed under the gantry head.

2.2 Data collection for electrons

The data collection procedure for electron beams included two major parts: measurements with and without applicators. There are four distinct measurements that need to be collected for each electron beam energy: air profiles, water depth dose curves, water profiles, and absolute dose measurements.

2.2.1 Air profiles

There are 6 MeV, 9 MeV, 12 MeV, 16 MeV, and 20 MeV electron beams installed in the Truebeam linear accelerator at the Dana Cancer Center. For each energy, air fluence profiles were scanned without applicators for both rectangular and square field sizes. Profiles were obtained by measuring two separate planes with 20 cm intervals between them; the first plane had an SDD equal to 75 cm, and the second plane was set to have an SDD of 95 cm.

Measurements were taken with field sizes of $8 \times 8 \text{ cm}^2$, $8 \times 20 \text{ cm}^2$, $8 \times 30 \text{ cm}^2$, and $30 \times 30 \text{ cm}^2$. For rectangular fields, the upper jaw (the y jaw in Truebeam machine) is fixed while the lower jaw (the x jaw) moves. The MLC leaves were retracted all the way back as far as possible in order to not block the actual field size. One additional parameter called relative output factor is also required for the air fluence profile, which is calculated by normalizing all readings from the detector with measurements for the $8 \times 20 \text{ cm}^2$ field size at 75 cm SDD. The figure below shows the configuration used for air measurements:

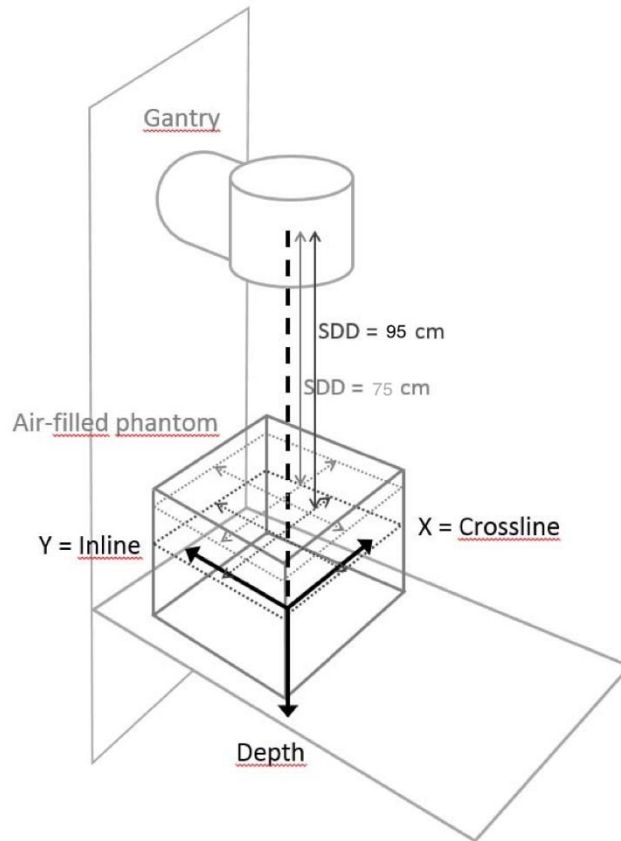


Figure 2-2: Open air profile measurements at 75 cm and 95 cm SDD

2.2.2 Open water depth dose

Depth doses were scanned in the water tank. The measurement was again obtained without any applicators present and with the field unblocked, which meant both jaws and the MLC leaves were retracted to the maximum allowable distance ($40 \times 40 \text{ cm}^2$). SSD was set to be 100 cm.

2.2.3 Water depth dose with applicators

There are several different sizes of applicators utilized clinically in the institution, including $6 \times 6 \text{ cm}^2$, $10 \times 10 \text{ cm}^2$, $15 \times 15 \text{ cm}^2$, $20 \times 20 \text{ cm}^2$ and $25 \times 25 \text{ cm}^2$. The settings of the gantry, the couch, and the collimator were all set to the values that were

used in the previous measurements (all angles were set to 0 degrees and SSD was set to 100 cm). Additionally, cutouts were mounted in applicators while collecting data. As an electron beam travels toward a patient, it will pass through components of the linear accelerator gantry, such as the scattering foil or the transmission ion chamber, as well as air; electrons can also interact with the collimator, applicators, and the patient, which leads to the production of bremsstrahlung radiation. For every energy and applicator size, depth dose curves measurements should be deep enough to contain the bremsstrahlung tail portion. Table 2-1 presents the minimum depth used to confirm the bremsstrahlung tail is included.

Table 2-1: Minimum depths for measuring the bremsstrahlung tail with distinct energy ranges.

Electron energy (MeV)	Minimum bremsstrahlung depth (cm)
$4 \leq E \leq 6$	5
$6 < E \leq 15$	10
$15 < E \leq 25$	15

Beam profiles for each energy and applicator were measured both within the high dose region (the shallow portion of the electron depth dose curve), and the region that lies beyond the maximum range of the electron beam. Typically, the electron loses about 2 MeV per cm in water. In order to make the process more convenient, the minimum bremsstrahlung depth was utilized for scanning the beam profile in the low dose region. Table 2-2 presents the shallow depth used for each energy range.

Table2-2: Shallow depths (high dose region) for beam profile measurement with different energy ranges.

Electron energy (MeV)	Shallow profile depth (cm)
$4 \leq E \leq 6$	1
$6 < E \leq 15$	2
$15 < E \leq 25$	3

Additionally, when scanning the beam profiles, it is crucial to measure regions outside of the field for at least 4 cm from each edge of the field to define the beam profile penumbra correctly.

2.3 Equipment used for measurements

All measurements were done in the $48 \times 48 \times 41 \text{ cm}^3$ Blue Phantom² water tank, manufactured by the IBA Dosimetry Corporation. Data was collected and processed with the OmniPro-Accept 7.4 software, also designed by the same manufacturer.

The detectors utilized for photon measurements were the Edge Diode, the A16 and the CC 13 ion chamber. Properties of these detectors are shown in the Table 2-3.

Table2-3: Detectors utilized for commissioning data

Detector name	Beam quality	Size	Field sizes
A16	Photons	Cylinder shape (height and width are 0.24 cm)	Small fields (3×3 , 5×5 , $7 \times 7 \text{ cm}^2$)
CC13	Photons, Electrons	Cylinder shape (height and width are 0.61 cm)	Large fields (photons: $\geq 10 \times 10 \text{ cm}^2$, electrons: all cone sizes)
Edge Diode	Photons	Flat shape (height and width are 0.03 cm)	All fields for 18MV

Importantly, the Edge diode cannot be used with electron measurements due to the lack of published documentations offering corrections and algorithms for transferring measured ionization curves to dose curves with shielded diodes.

2.4 Beam modeling

After importing all depth dose curves and beam profiles for each beam quality separately, the next step was beam modeling. The main purpose of this step is to match the shape of measured depth dose curves and measured beam profiles with computed curves from the treatment planning system software. This is extremely important to achieve accurate dose calculations.

2.4.1 Photon beams modeling

There are numerous parameters available to the user to adjust different portions of the computed curves. Beam modeling can be divided into two major parts: depth dose curve modeling and beam profile shape modeling. All parameters that can be adjusted to modify percent depth dose curves and beam profiles are listed in Appendix A. The following instructions show how to model and match the measured curves by adjusting representative parameters.

2.4.1.1 Auto-modeling

In the beginning, the auto-modeling process built into the treatment planning system was performed. Auto-modeling allows a quick run of the beam model data against the measured to initiate the process. Parameters of the auto model are typically coarse as shown in figure 2-3. Auto modeling includes the following steps:

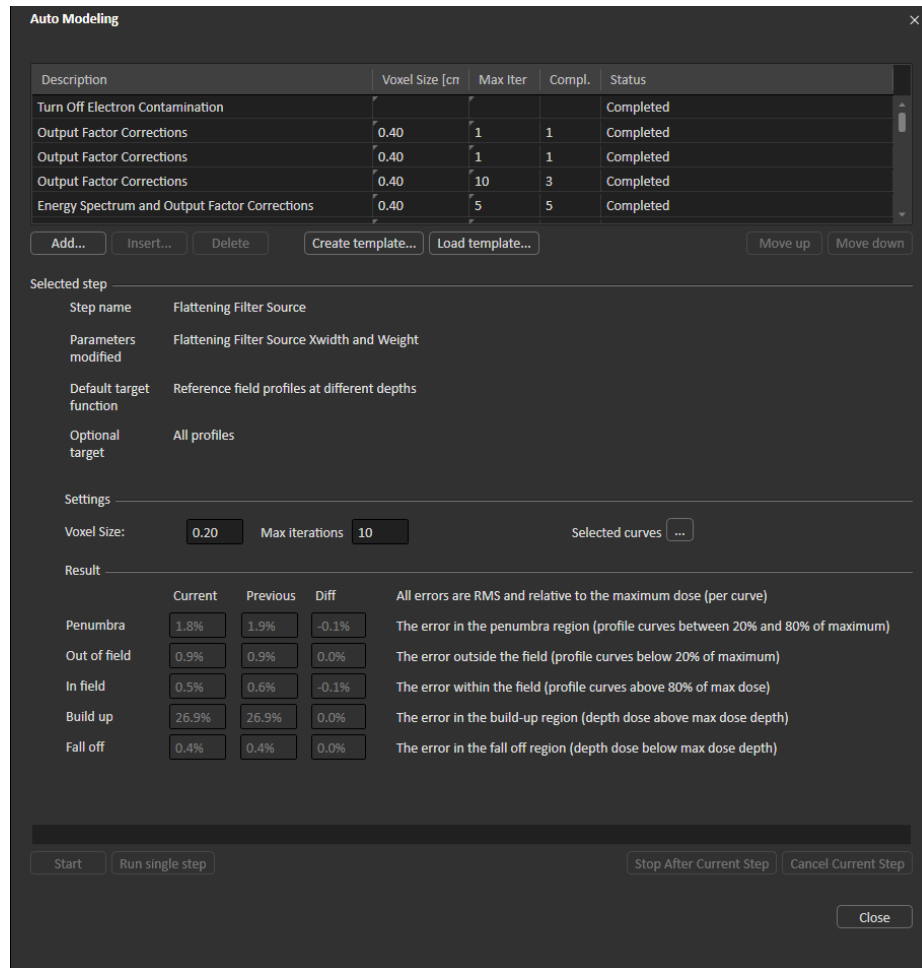


Figure 2-3: The operating window for the auto-modeling process

Step 1. Turn off electrons contamination (which affects the build-up region) – to avoid electrons contamination during the first modeling attempt. This function should be turned back on before starting following steps. One can turn on the electron contamination option to adjust the build-up region of percent depth dose curves. With the electron contamination off, one can start tweaking the computed percent depth dose curve to fit the measured data beyond the depth of maximum dose region by adjusting the energy fluence spectrum.

Step 2. Output factor corrections (fall-off region) – This factor corrects scattering into the monitor chamber, and it has to be re-optimized every time after adjusting other parameters which are related to scattering, such as the energy spectrum.

Step 3. Photon energy spectrum corrections (fall-off region) – Since the spectrum for every nominal energy consists of a number of monoenergetic values (an example of the spectrum is shown in figure 2-4), by adjusting the values of fluences for individual energy bins, the user can influence the final shape of the percent depth dose curve.

Increasing the weight of high energy photons in the spectrum will shift the whole PDD curve toward deeper depths. The main purpose of this step is to sculpt the shape of the fall-off region of the curve.

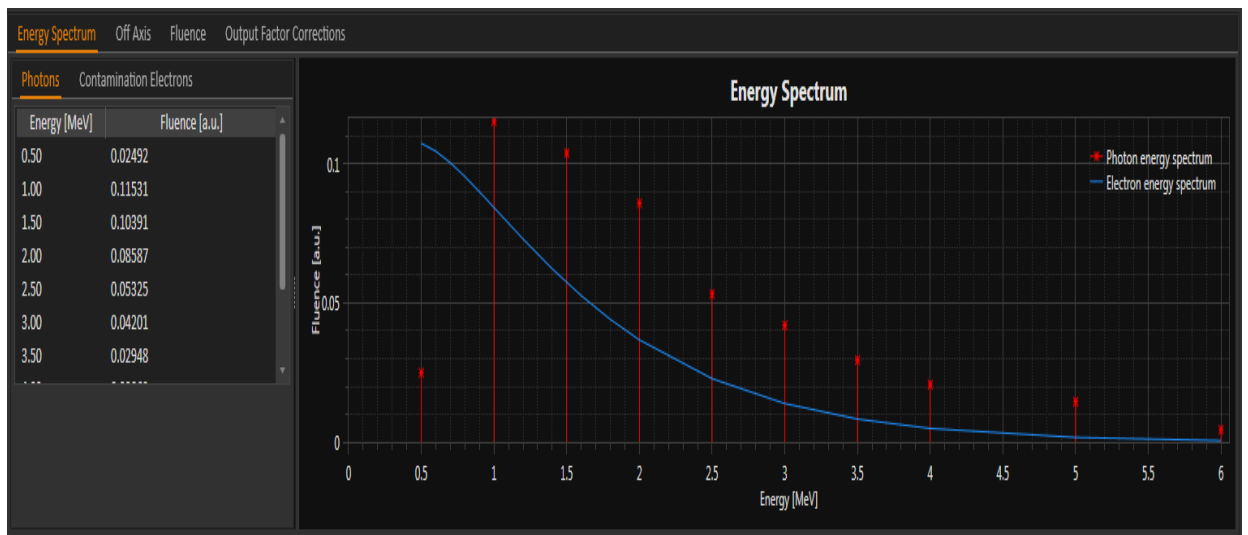


Figure 2-4: Energy spectrum for a regular 6 MV beam. The red lines represent the photon energy bins and the blue curve is the energy spectrum of the contamination electrons.

Step 4. Beam profile corrections (in-field region) – This correction factor helps symmetrize the beam profile with different radii. Increasing or decreasing the value at a specific radius can create a rise or a drop around that radius.

Step 5. Off axis softening (in-field region) – The off axis softening factor can be used to obtain a better fit for the beam profile. This parameter affects the profile in a manner similar to the beam profile correction parameter, but the response of the profile is less sensitive.

Once an acceptable match is achieved for the region of the PDD below d_m , the electron contamination can be turned back on to start modeling the curve within the build-up region, which represents the distance from the surface to d_m .

Step 6. Contamination electrons (build-up region) – The electron energy spectrum model is an exponential distribution (Eq. 1). Two components can be changed to tune the electron energy spectrum. The parameter E_0 determines the fall-off of the exponential curve, and the parameter C regulates the contribution of low-energy electrons.

$$\text{Fluence: } f(E) = E^C * e^{-E/E_0} \text{ [Eq. 1]}$$

2.4.1.2 Manual beam modeling

After running through the auto-modeling process, manual adjustments were performed. The following are some of the parameters that were manipulated most frequently during the modeling process:

- For PDD curves
 1. Energy spectrum – In general, this factor influences fall-off curves that are below

the depth of the maximum dose. For example, if the shoulder of the computed %DD curve is lower than the measured one, increasing the fluence of low-energy photon bins, such as 0.5 MV or 1 MV, can bring up the shoulder region (shown in the figure 2-5 below).

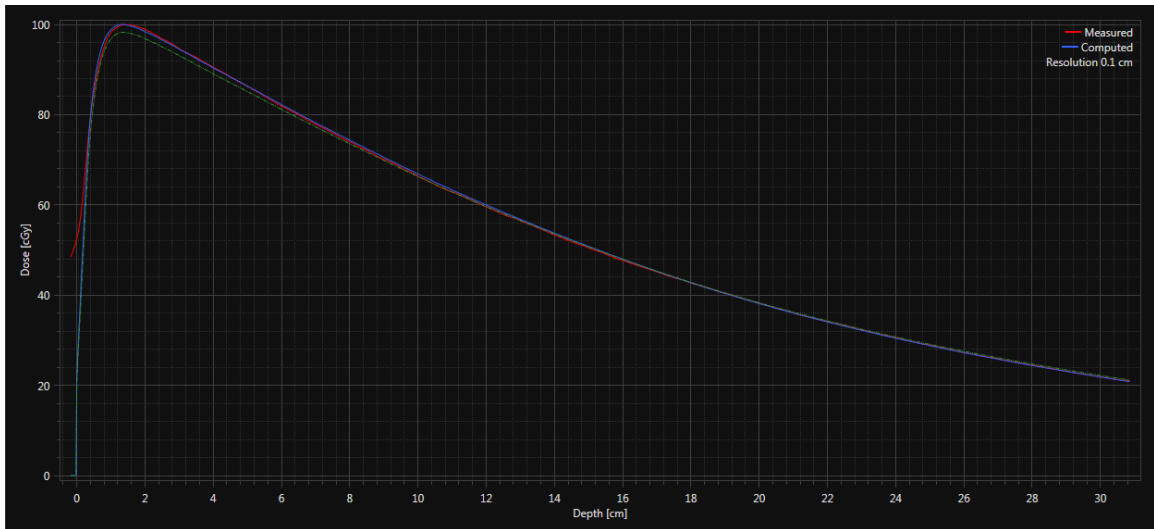


Figure 2-5: The 6 MV $10 \times 10 \text{ cm}^2$ field size PDD curve changes after increasing the fluence for the 1 MV energy bin. The red curve is the measured data; the green dashed curve is the former computed curve before modifying the energy spectrum, and the blue curve is the latest computed data. These colored curves represent the same thing in all RayStation figures.

2. Electron contamination – Increasing parameters C or E_0 slightly increases dose in the build-up region, the depth of d_m , and maximum dose simultaneously; this effect is presented in the figure 2-6. This affects the surface dose and the build-up region, and the effect is more obvious for large fields.

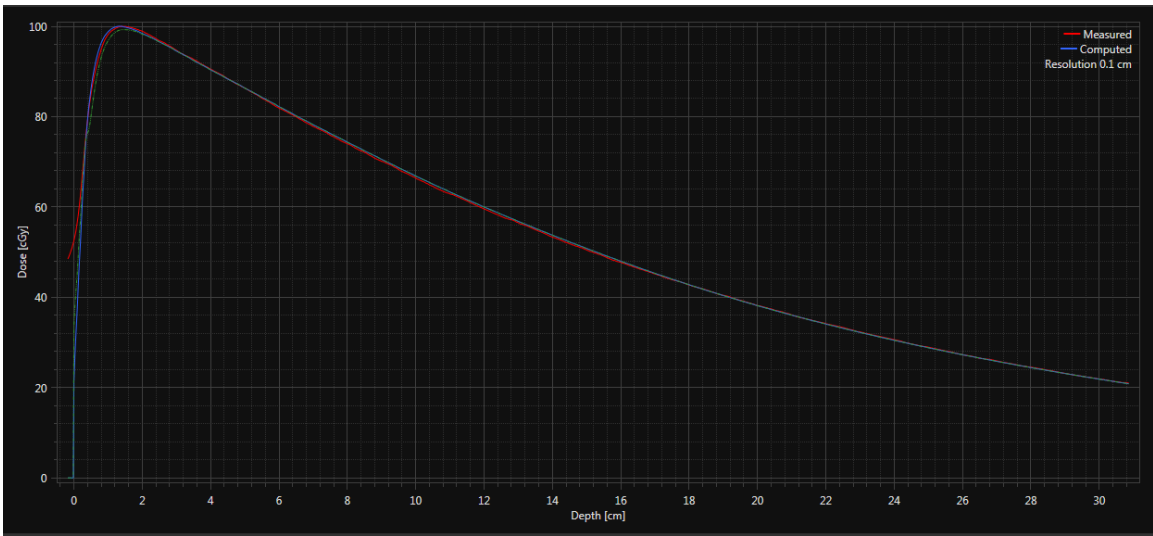


Figure 2-6: The 6 MV $10 \times 10 \text{ cm}^2$ field size PDD curve changes after increasing both C and Eo in order to achieve a more precise fit within the build-up region.

3. Fluence – The factors listed below are various adjustable parameters contained in this tab. A few parameters are not included in the auto-modeling script, such as the effective distance to source, transmissions, and additional MLC parameters; although these parameters can be modified manually, they should not differ dramatically from measured transmissions or known properties of hardware.
 - a. Effective distance to source – The effective distance to source is typed in for the flattening filter, y jaws, x jaws, and MLC. It represents the distance from the photon target to the collimator and the flattening filter. The collimator and the source are modeled without any extensions in the z direction, which means the thickness of the jaws, MLC, and flattening filter cannot be added to the model. The best way of making a reasonable approximation for the actual thickness is to enter the effective distance to source from the bottom of each component.

b. Flattening filter weight – This parameter is the proportionate contribution of the flattening filter source relative to the total photon source strength.

Increasing this weight will shift the whole PDD curve downstream. The sum of the two photon sources, including the weight of primary and flattening filter, is equal to 1. A representative is shown in figure 2-7.

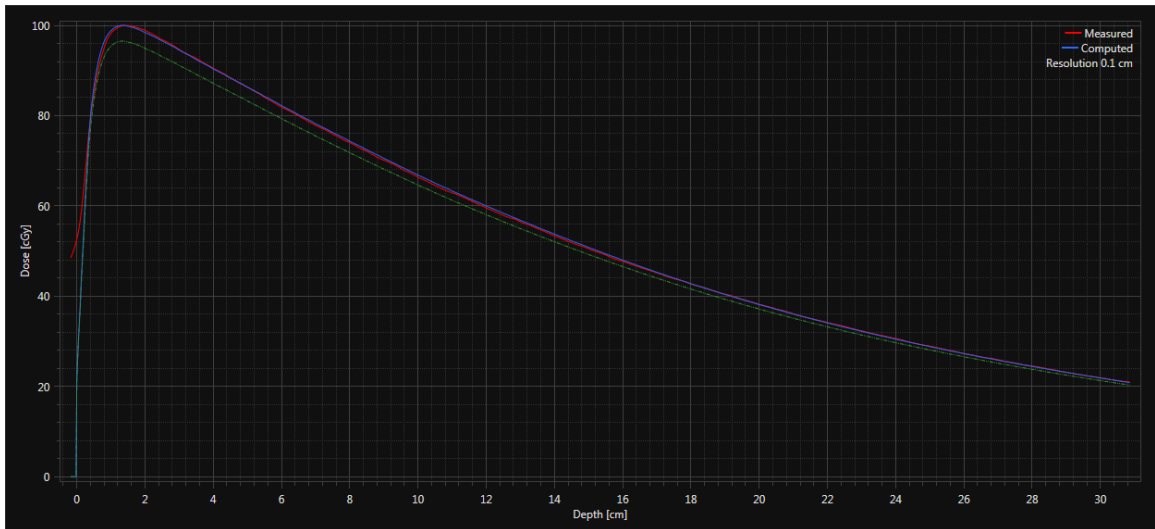


Figure 2-7: Decreasing the weight of the flattening filter source results in a lifting of the entire 6 MV $10 \times 10 \text{ cm}^2$ field size PDD curve to help it match the measured curve.

c. Electron source weight – The electron source weight is a relative strength comparing with two photon sources, which affects the build-up region of percent depth dose curves.

d. Weight of flattening filter electron source – This weight represents the fraction of total electrons that will be generated from the flattening filter.

- For beam profiles

- a. Primary source width size – The most effective parameter for reducing or increasing penumbras and horns in both the x and y directions. In other words, this factor alters the steepness of the penumbra region as shown in figure 2.8.

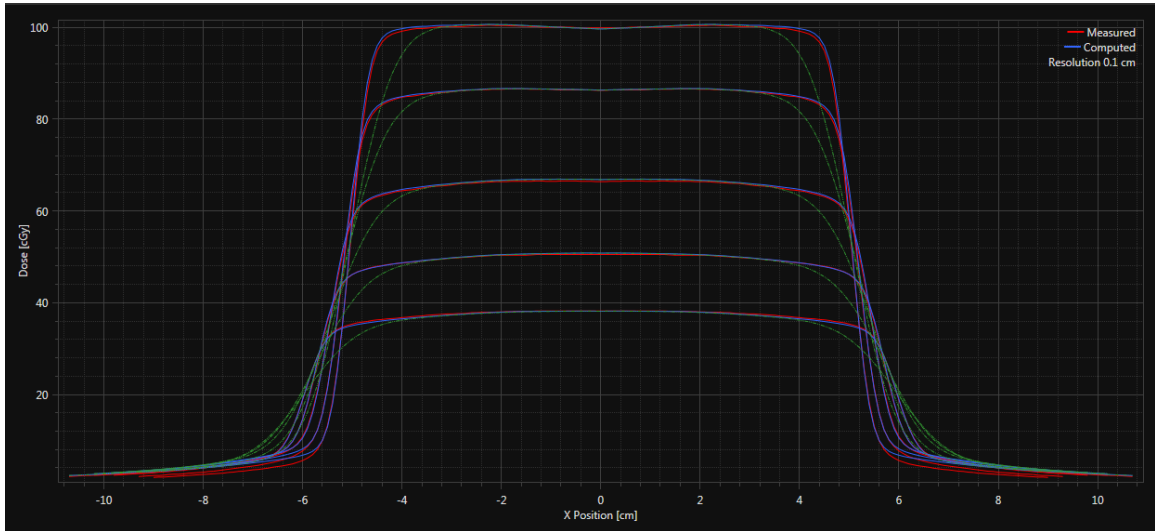


Figure 2-8: Increase the decline of the penumbra by decreasing the width of the primary source for a 6 MV beam with $10 \times 10 \text{ cm}^2$ field size at all depths.

- b. Flattening filter source weight – This also affects dose in the out-of-field region for beam profiles.
- c. Collimator transmission – Start with the measured value. The transmission factor can only be entered for x jaws and the MLC. The y jaws are modeled with zero transmission. Increasing transmission will increase the dose contribution outside of the field. A representative is shown in figure 2.9.

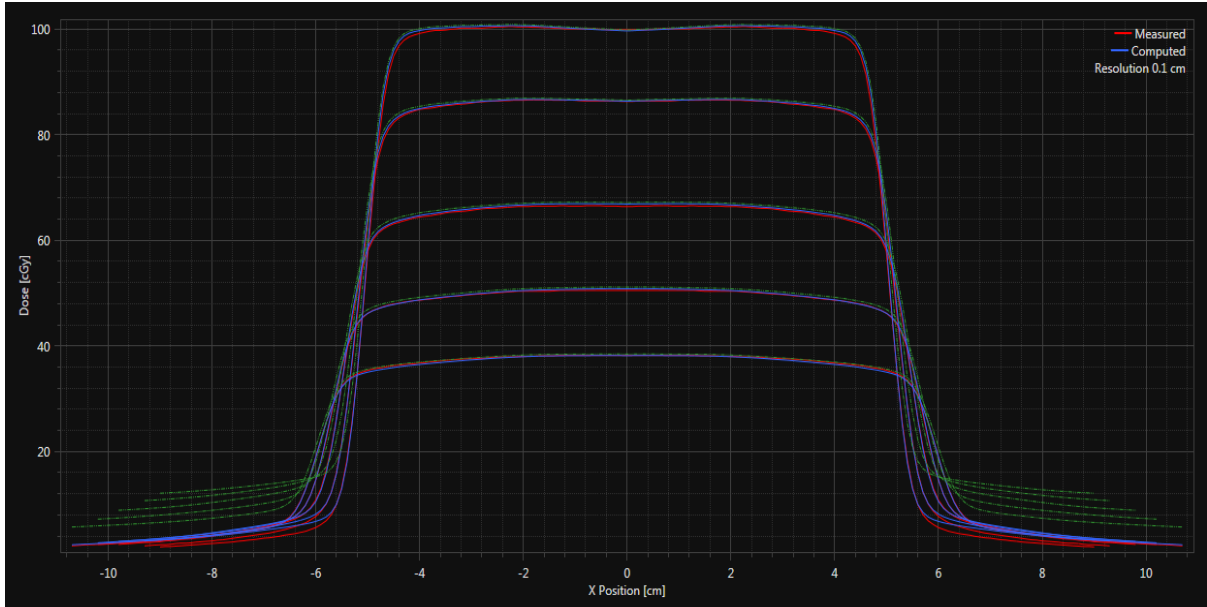


Figure 2-9: Decreasing the transmissions through the x jaw brings down the out-of-field x-direction profile for the 6 MV beam with $10 \times 10 \text{ cm}^2$ field size at all depths.

2.4.1.3 FFF beam modeling

The Procedures used to model FFF beams were similar to those used to model flattened beams, although there were a few distinct steps. First, there is a checkbox under the fluence tab that needed to be checked, which ensured settings were correct in the DICOM export. Second, all entries in the off axis softening table were set to zero since this parameter tweaks the beam profile based on the flattening filter, which was absent in the FFF beam model. Last but not least, the shape of the beam profile correction factors was expected to be gradually dropping from 1 at zero radius to close to 0 at the largest radius instead of the flat platform expected with conventional beams.

2.4.2 Electron beams modeling

It was useful to run the “optimize electron energy spectrum” option with the open field measurement in water to obtain reasonable initial parameter values as shown in figure 2-10 and figure 2-11.

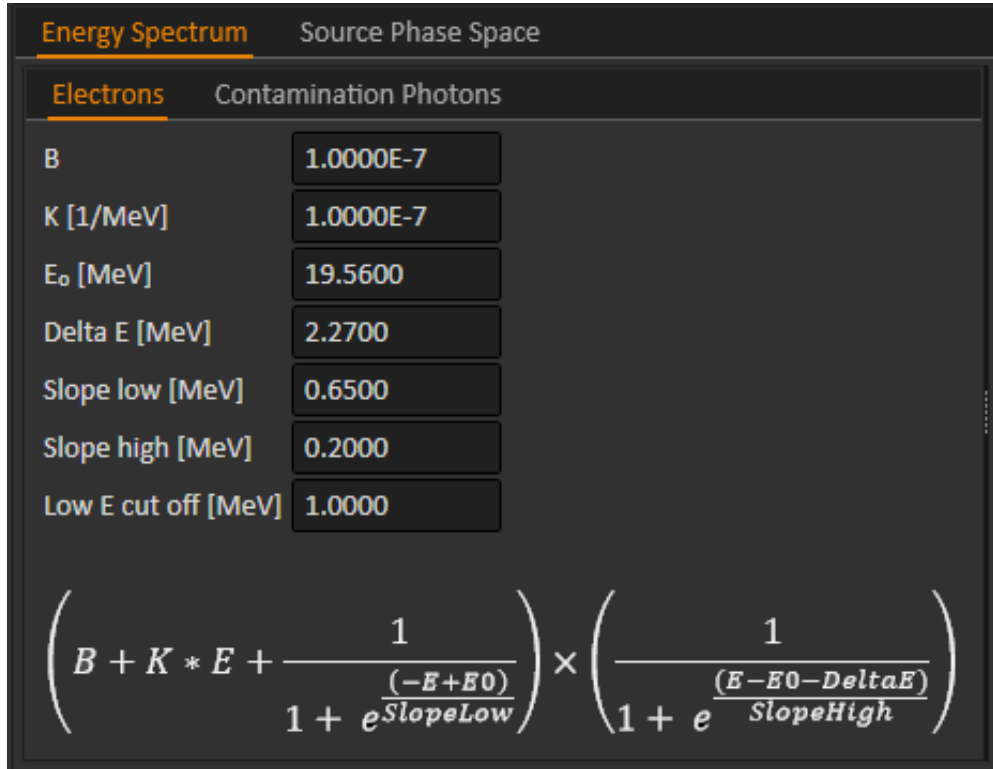


Figure 2-10: Example of parameter values for describing the electron energy spectrum for a 20 MeV beam.

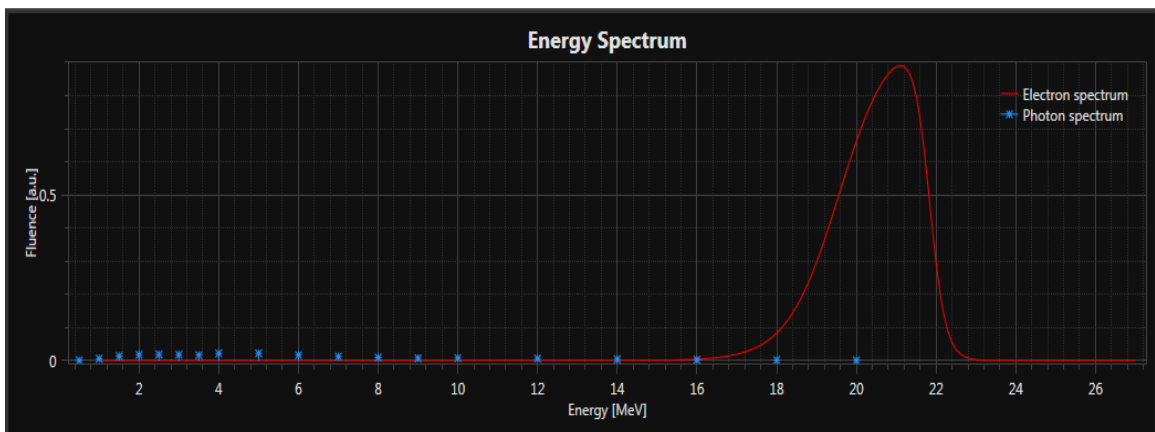


Figure 2-11: The electron energy spectrum for 20 MeV modeled by the parameters found in figure 2-10. The red line represents electrons and blue energy bins represent contamination photons.

The form of the energy spectrum of electrons from the time they depart from the scattering foil is given by the equation 2.

$$\left(B + K * E + \frac{1}{1 + e^{\frac{(E_0 - E)}{SlopeLow}}} \right) \times \left(\frac{1}{1 + e^{\frac{(E - E_0 - DeltaE)}{SlopeHigh}}} \right) \quad [\text{Eq. 2}]$$

1. B: constant that describes the low energy tail of the energy fluence. This parameter is capable of determining the height of the low-energy tail in the spectrum. In other words, the B constant affects the entrance dose, the build-up region, and the depth of the maximum dose on the percent depth dose curve.
2. K: the linear coefficient. Increasing this value will bring up the steepness of the low-energy tail in the spectrum, which brings down the entire PDD curve, especially at the low dose region.
3. E_{cut} : low energy cutoff. Electrons below this energy won't be taken into account for final dose calculation.

The above three parameters influence the build-up region of the PDD curve and the surface dose.

4. E_0 : the parameter value is close to the nominal beam energy. This represents the middle point of the rising part of the fluence spectrum. Changing this values shifts the whole energy fluence spectrum left or right horizontally.

5. Delta E: this factor determines the width of the electron energy spectrum. This can be modified to fit the shoulder region of the PDD curve, but it also slightly shifts the PDD fall-off region horizontally, so delta E is often changed with E_0 to get a good match for the PDD beyond d_m . An illustration of this is shown in the figure 2-10.

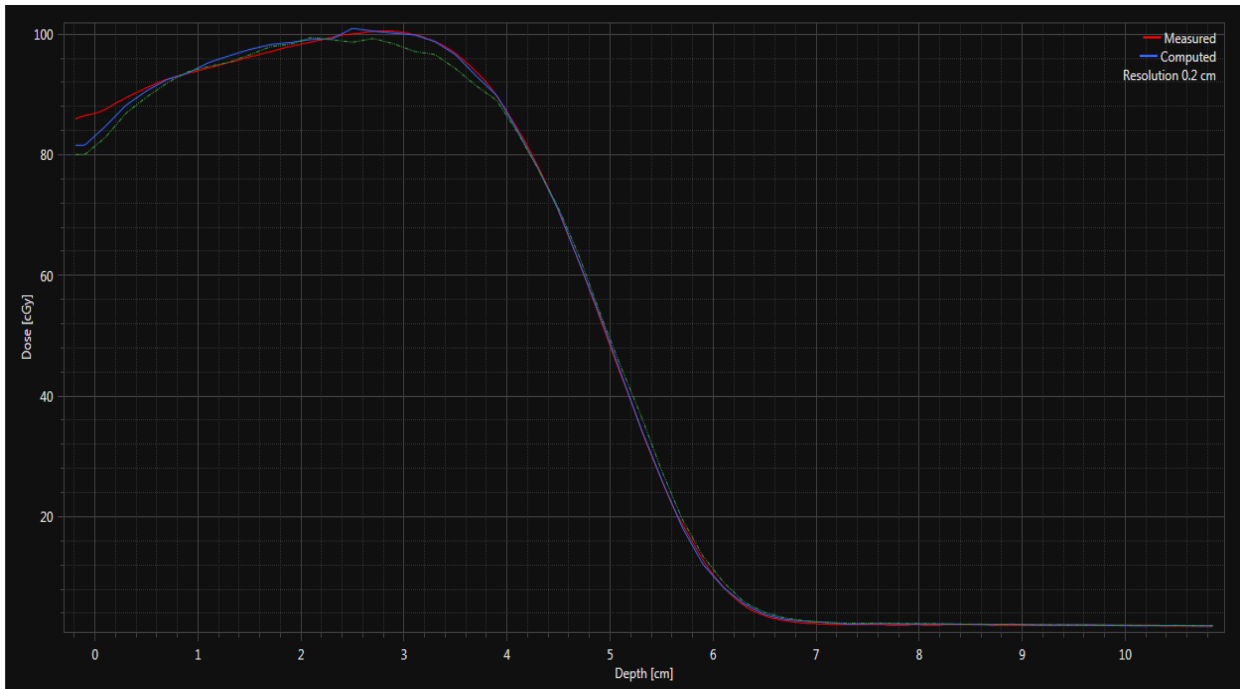
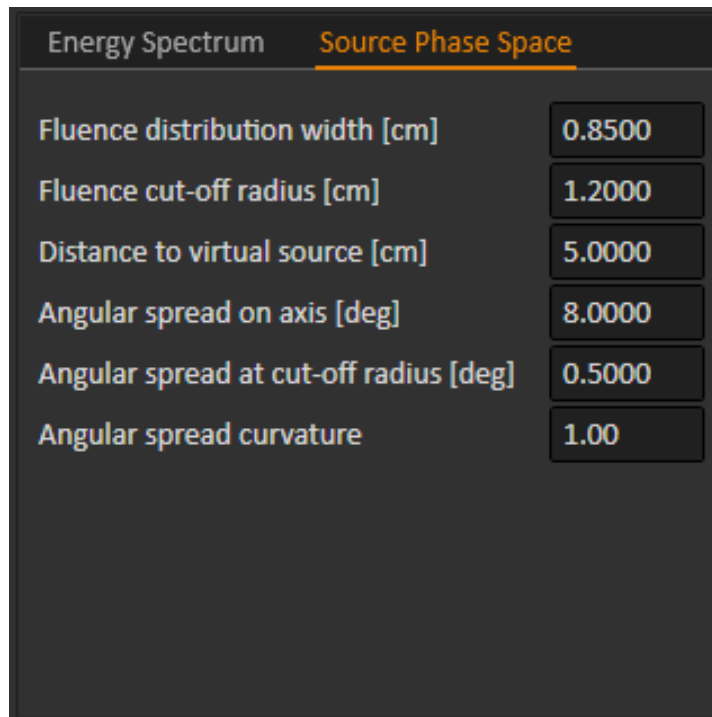


Figure 2-12: Increasing delta E to raise the shoulder portion and decreasing E_0 to shift the fall-off portion to a shallower depth for fitting the computed PDD curve with the measured 12 MeV electron PDD curve.

6. Slope high and slope low: these two elements determine the steepness of the ascending part and the descending part of the energy spectrum respectively. Areas under either the low-energy side of the peak or the high-energy side of the spectral peak can be reshaped to affect the fall-off region of PDD curves.

Next section went to the contamination option, and all adjustable parameters are listed in the table A-2. The first optimization with the open field measurement can be used to establish reasonable values for these factors. Contamination photons contribute doses to the deep region mostly, so the measurement depth should be set to a point within the bremsstrahlung tail of the PDD curve.

After successfully modeling PDD curves, computed beam profiles needed to be matched with measured ones as well. Figure 2-13 lists all parameters found under the source phase space tab for tuning profiles. Table A-2 contains geometric descriptions for each component; figure 2-14 offers an illustration that graphically describes the role of each parameter.



Energy Spectrum	Source Phase Space
Fluence distribution width [cm]	0.8500
Fluence cut-off radius [cm]	1.2000
Distance to virtual source [cm]	5.0000
Angular spread on axis [deg]	8.0000
Angular spread at cut-off radius [deg]	0.5000
Angular spread curvature	1.00

Figure 2-13: Parameters capable of modifying the 20 MeV electron beam profile.

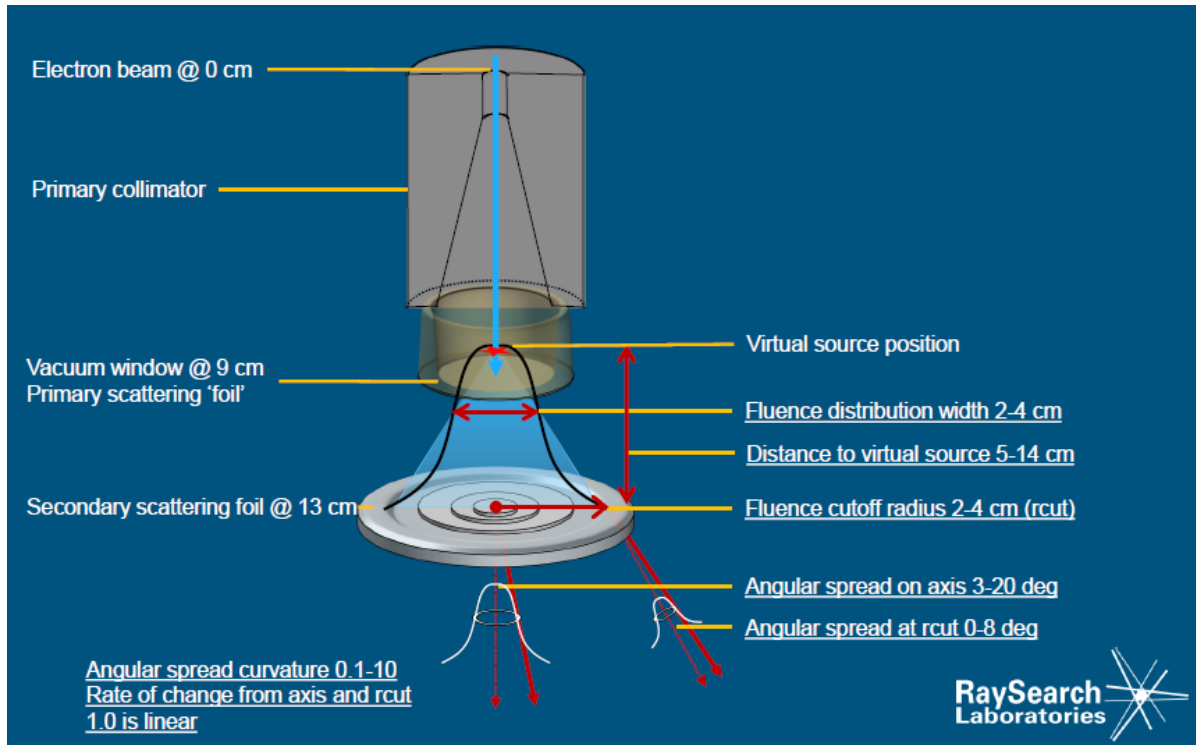


Figure 2-14: Functions of individual parameters involved in electron beam profile modification

The following cases provide solutions for some common problems encountered during the electron beam profile modeling process.

- a. Difficulty: The shoulder of the computed profile was below that of the measured one.

Solution: Reducing the angular spread angle at the cut-off radius can direct more electrons to the edge of the secondary scattering foil and heighten the shoulder of the beam profile.

- b. Difficulty: Horns appeared on the large field size beam profile.

Solution: Increase the angular spread at the cut-off radius or decrease the fluence distribution width will diminish horns.

- c. Difficulty: Computed air profiles were not corresponding with measured ones after obtaining a good fit for curves with applicators.

Solution: The most important goal for beam modeling is to acquire good agreement between measured applicator curves and computed ones since these curves are going to be utilized during patient plan dose calculations. Air profiles are useful to obtain starting values for source phase space parameters.

Additionally, there are two parameters that can be adjusted individually for different cone sizes. First, the indirect electron weight correction factor, which contains a function that, if the computed dose does not match the measured dose in the region from the surface to d_m , has a strong effect on raising or lowering the computed curve within this specific zone. Next, electron dose normalization, which can be adjusted to re-normalize the entire PDD curve upstream or downstream.

2.5 Point dose measurements for verification

After final matches for PDDs and beam profiles were reviewed and approved by certified medical physicists, several point dose measurements were made using both the ArcCHECK phantom and a water tank and compared. Since modeling results for electrons has not been reviewed by any certified medical physicists yet and requires a distinct way to do dosimetric tests, it is work in progress at the time of this writing and subsequent validations were implemented particularly for photons.

2.5.1 Point dose measurements in homogeneous and inhomogeneous media

In this section, the ArcCHECK phantom with A16 type ionization chamber inserted, which is clinically used for treatment plans quality assurance, were used for dose measurements. The ArcCHECK phantom has inserts with various density materials (lung, muscle and titanium) that can be put in or out for different purposes. First, the CT image of the phantom with an ionization chamber inserted was imported into the treatment planning system. To create an inhomogeneous environment, material of inserts above or below the detector were overwritten to either lung, muscle or titanium for any specific situations. Next, placing an AP beam with 6 MV energy and jaw-defined $10 \times 10 \text{ cm}^2$ field size at 100 SAD, and 200 MU/fx was delivered for each configuration. For the homogeneous data, all inserts made by PMMA were in the phantom for the computation. Recording the calculated point dose at the center of the sensitive volume of the ionization chamber from RayStation, and an example of the beam setting for the homogeneous measurement is shown in figure 2-15. As a next step, inserts above or below the chamber needed to be done to test point doses in the inhomogeneous medium, so identical procedures for recording the point dose at the central axis were repeated with different materials inserted. In the end, we placed an offset point 2 cm next to the isocenter (the tip of the ionization chamber) horizontally in RayStation for testing off-axis point doses.

Later, we set up the ArcCHECK phantom with ionization chamber inserted under the LINAC treatment head and aligned the phantom with the laser coordinate to ensure the sensitive volume of the ionization chamber was at the machine isocenter. Then all measurements were completed with different patterns of material replacement.



Figure 2-15: Beam arrangement and dose distribution in RayStation with PMMA inserted.

2.5.2 Point dose measurements in the water tank

The dosimetric tests described above were performed also in the same water tank used for collecting the commissioning data. Square field ($10 \times 10 \text{ cm}^2$), rectangular field ($5 \times 20 \text{ cm}^2$) and irregular field (L-shape), as shown in Figure 2-16, were designed for measurements. The cross-calibrated edge detector diode (Sun Nuclear Corporation) was utilized to measure point dose. All data were obtained with jaw-and-MLC-collimated fields. Central axis point dose measurements at d_m , 5 cm and 10 cm depth were required for all kinds of field size configurations. Off-axis point dose measurements were attained for the rectangular field along cross-line (2.75 cm and 7.75 cm from the CAX) and in-line (11 cm and 16 cm from the CAX) directions at 10 cm depth. For the L-shape field, extra measurements such as point dose measurements at the edge and the corner of the block were accomplished.

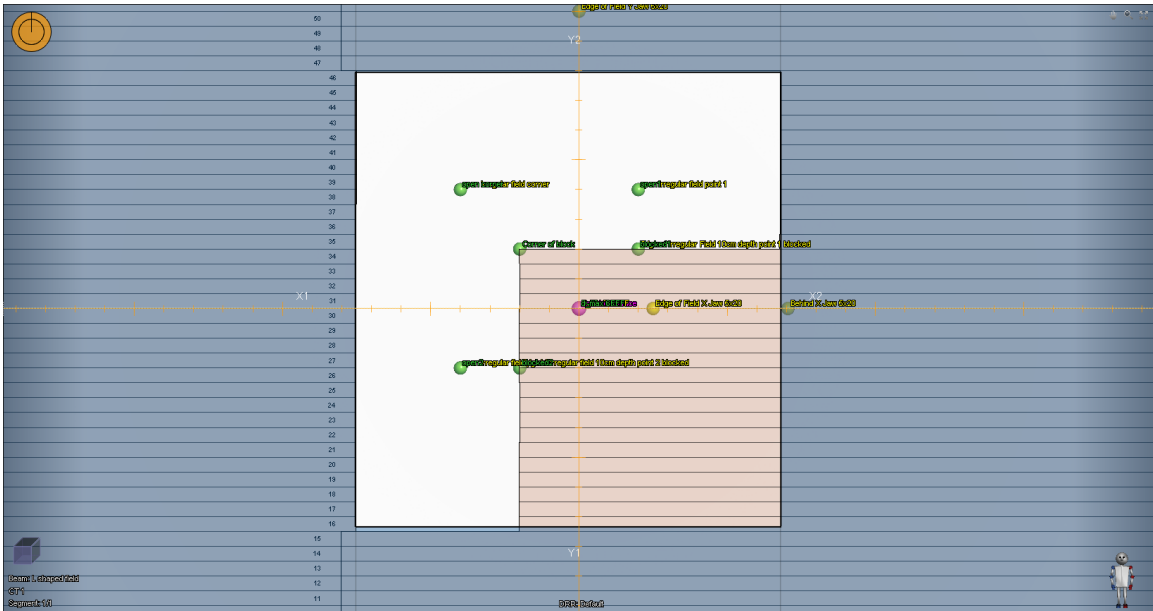


Figure 2-16: The irregular field (L-shape).

In consideration of purpose of verification, identical set-ups were built in RayStation TPS to calculate dose at particular point.

2.6 Treatment plans comparison for validation

Former approved and delivered treatment plans produced in Pinnacle TPS were imported to RayStation TPS, including a 3D whole brain plan, an IMRT mediastinum and lung cancer plan and a VMAT prostate cancer plan. Generating new plans with same beam arrangements and control points, and DVHs for PTVs as well as normal structures were compared.

Chapter 3

Methods and materials for the feasibility of using FFF beams to deliver conventional flat beams

3.1 General concepts of using FFF beams to deliver flat beams

After the Raystation treatment planning system was successfully commissioned and available to be operated clinically, this treatment planning software can be used to generate plans for dosimetric comparisons. The multi-leaf collimator has been introduced and widely used in the field of radiation therapy for a long time. Numerous functions of the multi-leaf collimator are important for generating a reasonable treatment plan, including conforming the dose distribution to match the irregular shape of the target, blocking hot spots in targets to make the dose distribution in the volume more uniform, and also creating different outlines of radiation fields. Observing the dissimilarities between radiation beams with and without the flattening filter, major differences will be higher doses around the central axis and dramatic dose fall-off from the center to the edge of the field for flattening filter free beams. However, MLCs are capable of modulating the dose distribution within the radiation field. If a uniform dose distribution can be achieved by the flattening filter free beam with the help of MLCs in delivering sliding window plans, the need to include the flattening filter in the linear accelerator might not

exist anymore. In order to carry out the practicability of the concept that the flattening filter is no longer needed in the head of the modern treatment units, beam profiles generated from open-field flat beams and flattening filter free beams which were forced to become flat using the sliding window technique and results were compared in this study.

3.1.1 Methods and materials

Beams with 6 MV energy was performed throughout this study due to the reason that TrueBeam machine contains only 6 MV for both with and without the flattening filter. A $50 \times 50 \times 50 \text{ cm}^3$ water cube image was imported into Raystation TPS. For the conventional flat beam, which has the flattening filter present, AP beams with open square field sizes (10×10 , 20×20 , $30 \times 30 \text{ cm}^2$) defined by jaws and MLCs were performed. SSD was set to 100 cm.

To continue, since a structure was necessary for optimizing an IMRT plan, meaning the sliding MLCs can be operated during irradiation, 0.1 cm thick planes with areas equal to corresponding field sizes were created at 10 cm depth from the water surface. The center of each plane was prescribed to receive 100 cGy for normalization.

The optimization parameter “uniform dose” was used to guide the TPS to achieve the goal by MLCs sliding within the field. After successfully producing uniform dose distribution on the plane, the “line dose” tool in RayStation was applied. With this tool, a line can be drawn across any regions of interest to obtain the beam profile along the line. In this case, profiles across the central axis and vertical to the sagittal plane of the water cube at 10 cm depth for different sizes of plane structures were gathered for data analysis.

The formula below was utilized to quantify uniformities:

$$\text{Percentage Uniformity} = \left(1 - \frac{\text{Standard deviation}}{\text{Average dose}}\right) \times 100 \text{ [Eq. 3]}$$

3.2 Main purposes for clinical treatment plans comparison

Since conclusions of the previous research already indicated out that it is workable to deliver a conventional flat beam with a FFF beam, this consecutive project intends to confirm the usefulness when applying to actual clinically approved treatment plans. By comparing doses that contribute to abutting normal structures with the same PTVs coverage, the attempt is to verify that it is feasible to create an identical or even higher quality of plans with flattening filter free beams.

3.2.1 Methods and materials

Ten patients were selected in this dosimetric comparison study, and all treatment plans were completed in Pinnacle treatment planning system. All plans were approved by radiation oncology specialized physicians and used as practical treatment plans for doses delivery in the University of Toledo Dana Cancer Center. Five patients with the head and neck cancer and five patients with the lungs and mediastinum cancer were involved. Every chosen plan was accomplished by operating several conventional 6 MV flat beams with the step-and-shoot IMRT technique. In order to undergo the comparison of plans, the second plan for each case was produced with 6 FFF beams. For plans having only one dose level of the PTV, the coverage of the PTV was achieved to be identical to each other. For plans involving more than one PTV dose level, such as two or three PTVs, they were complemented with the same coverage of one of the PTVs and higher coverages of other PTV levels.

For PTVs in head and neck cancer treatment plans, they were prescribed 6250 cGy to a high dose level, 6000 cGy to a medium dose level and 4500 cGy to a low dose level, however, only one patient was absent with the medium dose level involved. Adjacent critical normal structures are numerous, including the spinal cord, left and right parotids, the esophagus, the mandible, left and right submandibular glands, the larynx, and the oral cavity.

For PTVs in lung and mediastinum cancer treatment plans, two dose levels with different values were prescribed by physicians in four patients, and only one dose level existed in one patient. The distinct dose levels for patients respectively are listed in the table below:

Table 3-1: Dose levels for individual head and neck cancer patient

Group 1 (head and neck cancer patients)	PTV 1 (cGy)	PTV 2 (cGy)	PTV 3 (cGy)
Patient 1	6250		4500
Patient 2	6250	6000	4500
Patient 3	6250	6000	4500
Patient 4	6250	6000	4500
Patient 5	6250	6000	4500

Table 3-2: Dose levels for individual lung/mediastinum cancer patient

Group 2 (lung/mediastinum cancer patients)	PTV 1 (cGy)	PTV 2 (cGy)
Patient 1	6250	4500
Patient 2	4000	3000
Patient 3	6250	4500
Patient 4	4500	
Patient 5	6000	5400

During the optimization for FFF beams, an additional parameter “uniform dose” was added to eliminate hot spots in the PTV region, which did not often require to use for the flat beam; majority of other objectives and constraints utilized remained unchanged, some extra objectives were put in to meet demand of the equivalent coverage of PTVs.

To evaluate final results, average differences of maximum doses, mean doses, volumes receiving low percentages of the prescription dose for organs at risk between plans with FFF beams and with flat beams were elected. The idea of choosing the low-dose level irradiation to normal structures for investigation came from the knowledge that the greatest advantage of the FFF beam against the conventional flat beam would be a steeper dose fall-off beyond the PTV, therefore less doses contribute to normal tissues is expected to see in results.

Chapter 4

Results and discussions for commissioning the RayStation TPS

4.1 Beam modeling results

The final beam models for both photons and electrons with different field sizes and applicator sizes resulted in a good match with measured data in RayStation. In order to validate the decency of all fitted curves, the “curve quality” value was used to evaluate each model.

For PDD data, the curve quality was computed for both the build-up region (the region from the surface to the d_m) and the fall-off region (the region from the d_m to the end of the curve).

For beam profiles, the curve quality was calculated for the in-field region (between the left and right penumbra), the penumbra region (between the radius corresponding to 80% of the maximum dose and the radius corresponding to 20% of the maximum dose), and the out-of-field region (outside of the penumbra).

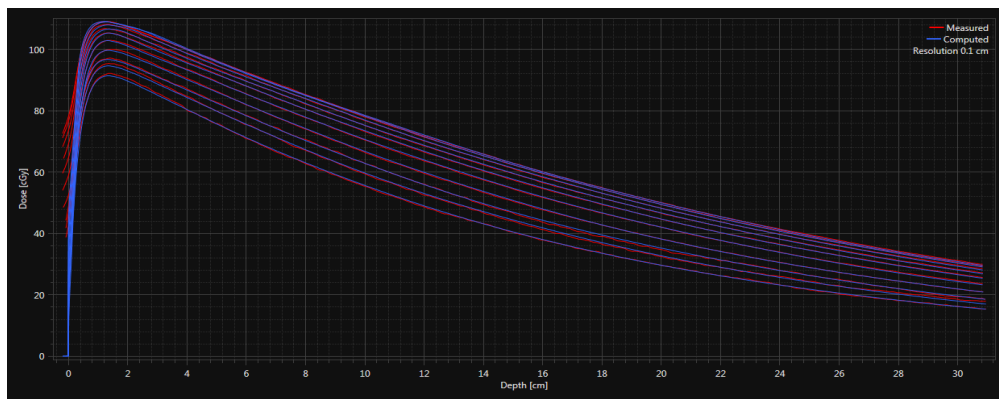
The curve quality value is the RMS difference between measured data and computed data, which can be described by the following equation:

$$\text{RMS} = \sqrt{\frac{1}{N} \sum_{i=1}^N \left(\frac{\text{computed dose} - \text{measured dose}}{\text{maximum dose for measured curve}} \right)^2} \quad [\text{Eq. 4}]$$

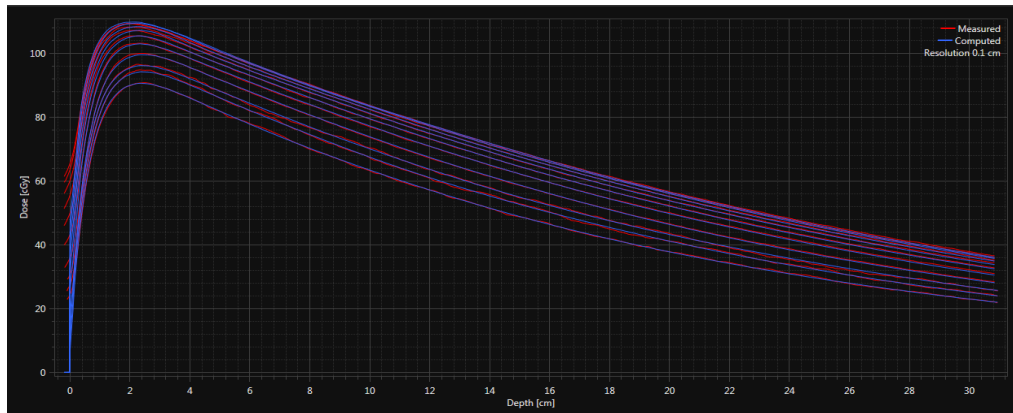
Where N is the total number of points included in the related region.

4.1.1 Photons

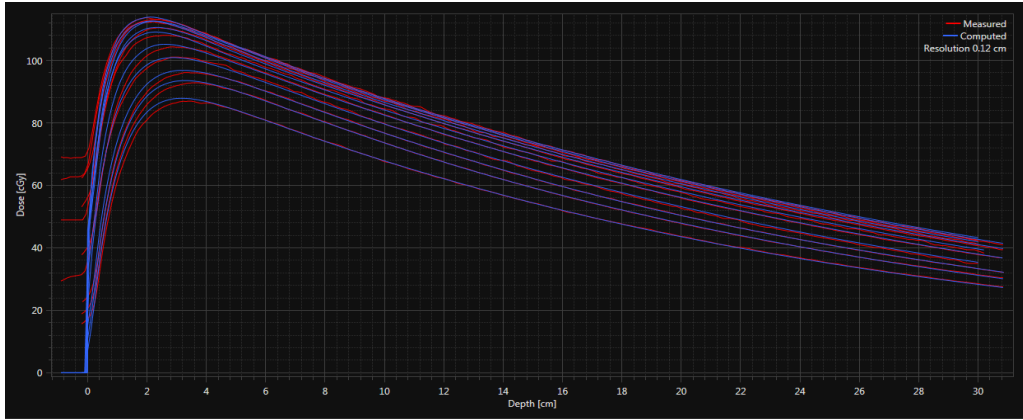
Final PDDs and profiles for each energy are presented in figure 4-1. Overall, the computed curves were in good agreement with measured curves.



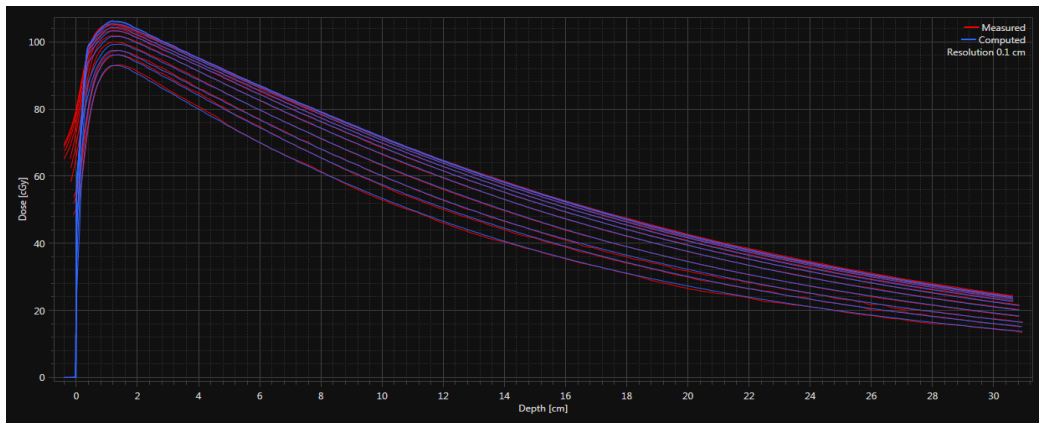
(a)



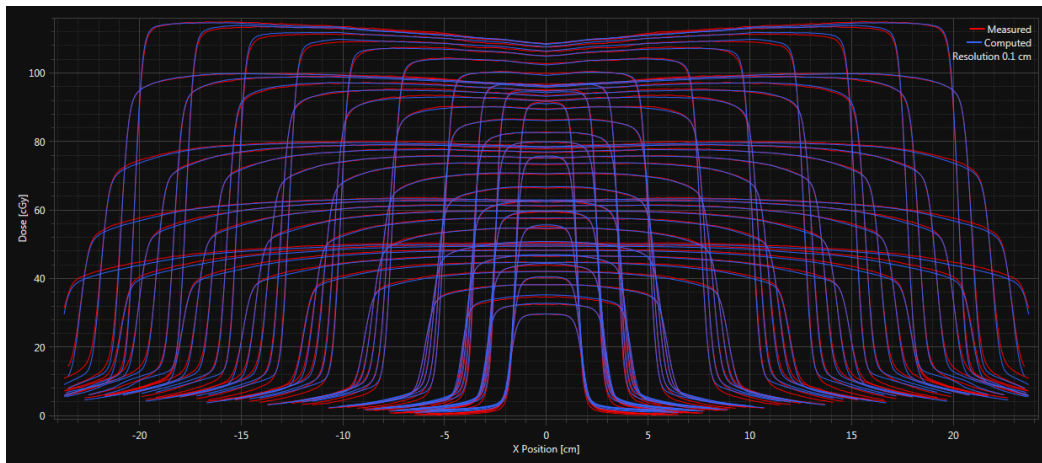
(b)



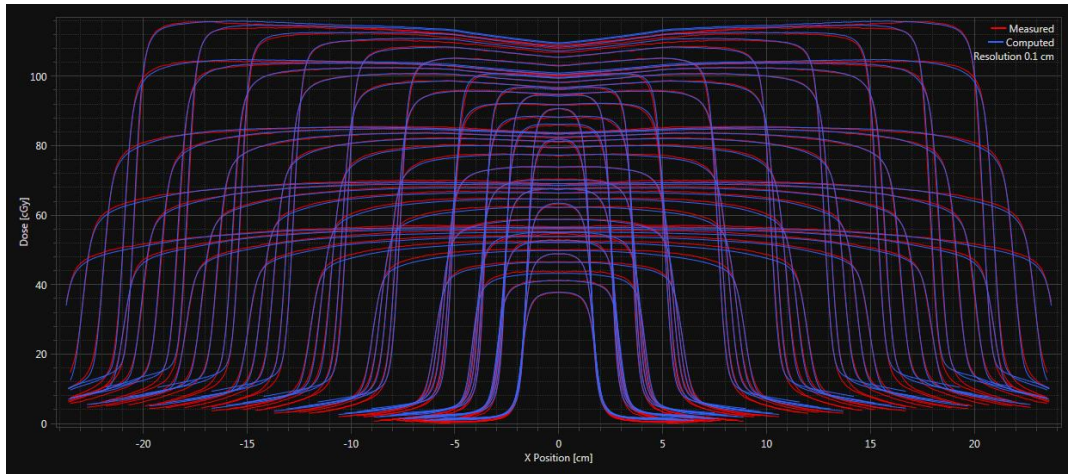
(c)



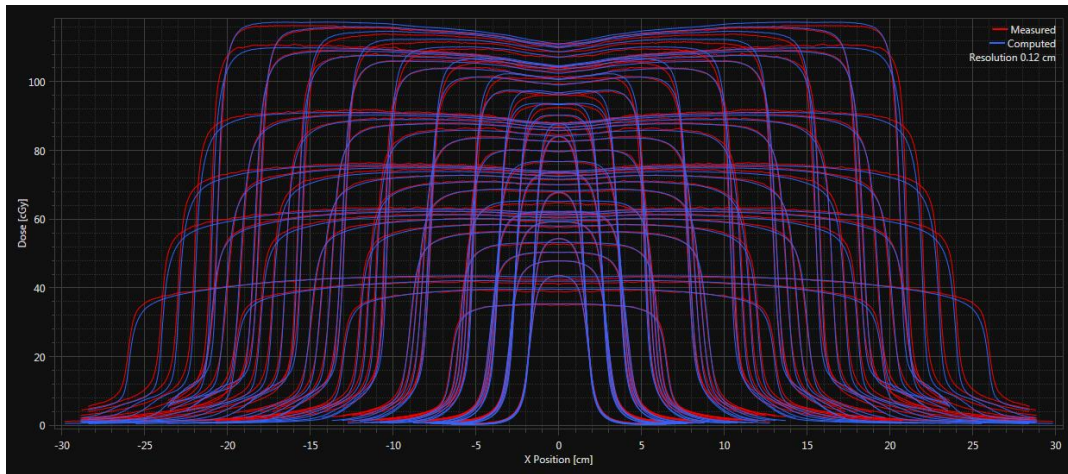
(d)



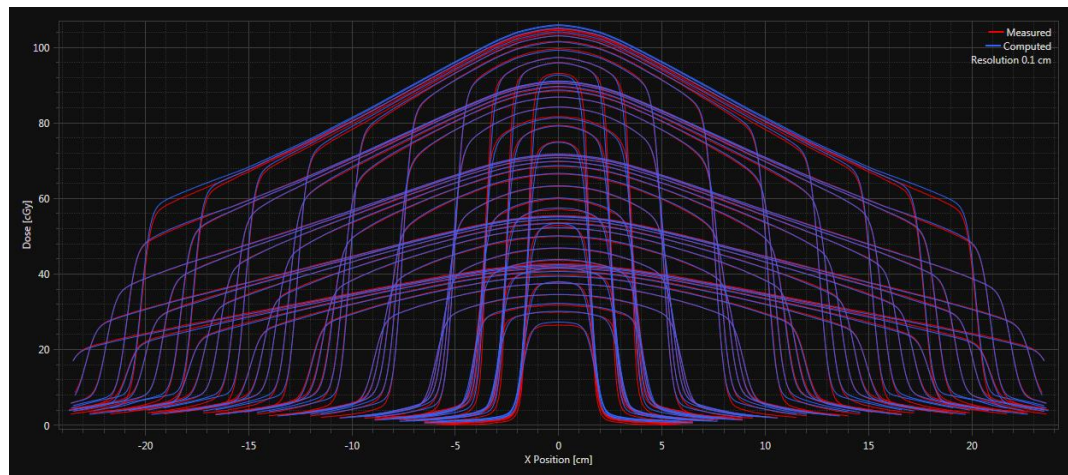
(e)



(f)



(g)



(h)

Figure 4-1: Final PDD curves for (a) 6 MV, (b) 10 MV, (c) 18MV, and (d) 6 FFF with all field sizes and cross-plane beam profiles for (e) 6 MV, (f) 10 MV, (g) 18MV, and (h) 6 FFF at all depths demonstrates the close fits between computed data (blue lines) and measured data (red lines).

Following the approach by Bongile, M et al., all percentage differences were divided into three categories: the small field size (≤ 5 cm), the medium field size (5 cm ~ 15 cm) and the large field size (>15 cm), and then took the average of quality values for each group with all depths (d_m , 5, 10, 15, and 20 cm) included; overall results are shown in the table 4-1.

Table 4-1: Analysis of average fit qualities and standard deviations (± 2 STD) for (a) PDDs, (b) cross-plane profiles and (c) in-plane profiles.

(a)PDDs	6 MV		10 MV		18MV		6FFF	
	Build-up* (%)	Fall-off (%)						
FS \leq 5cm	14.1 \pm 0.0	0.4 \pm 0.1	6.4 \pm 0.3	0.3 \pm 0.1	5.8 \pm 0.2	0.2 \pm 0.0	15.4 \pm 0.0	0.4 \pm 0.1
5cm < FS \leq 15cm	18.3 \pm 3.2	0.3 \pm 0.1	9.7 \pm 2.0	0.3 \pm 0.1	10.7 \pm 3.6	0.2 \pm 0.1	21 \pm 3.9	0.2 \pm 0.1
FS > 15cm	25.8 \pm 1.6	0.2 \pm 0.0	16.5 \pm 1.4	0.2 \pm 0.0	24.3 \pm 8.1	0.3 \pm 0.0	33.7 \pm 4.3	0.2 \pm 0.1

*Since all measured photon PDD data were collected with the detector moving from 30cm below the water surface (0 cm) to a position slightly above the water surface (-0.2 cm), the doses upon the surface were not calculated in the system, which resulted in a huge percentage difference between two curves.

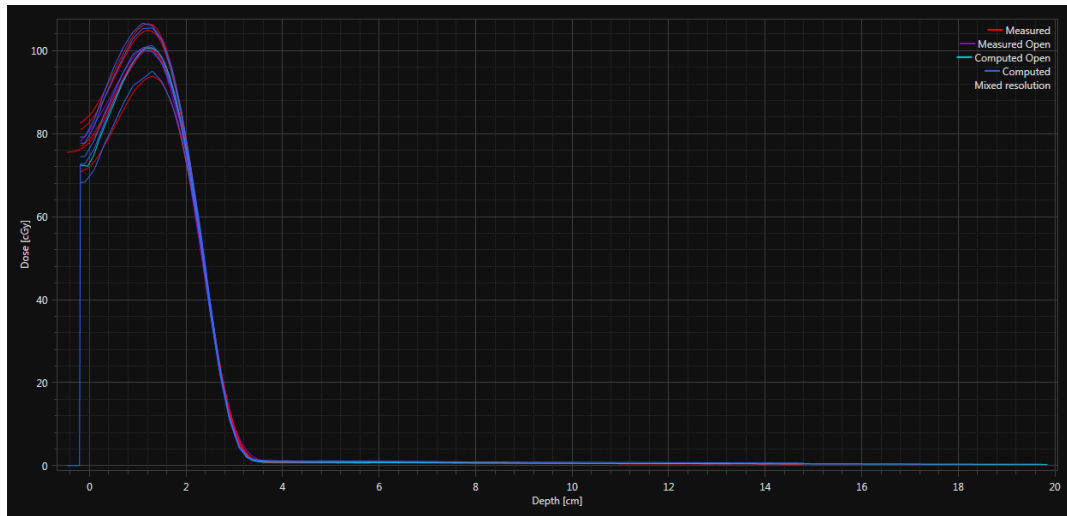
(b)Cross-plane Profiles	6 MV			10 MV			18MV			6FFF		
	In-field (%)	Penu mbra (%)	Out-of-field (%)	In-field (%)	Penu mbra (%)	Out-of-field (%)	In-field (%)	Penu mbra (%)	Out-of-field (%)	In-field (%)	Penu mbra (%)	Out-of-field (%)
FS \leq 5cm	0.6 \pm 0.4	2.3 \pm 0.7	1.6 \pm 0.5	0.5 \pm 0.3	1.4 \pm 1.0	1.4 \pm 0.4	0.9 \pm 1.0	0.9 \pm 0.6	0.7 \pm 0.6	2.3 \pm 1.2	5.2 \pm 1.0	1.8 \pm 1.0
5cm < FS \leq 15cm	0.5 \pm 0.6	1.3 \pm 1.5	0.9 \pm 0.7	0.7 \pm 0.9	1.4 \pm 0.9	1.5 \pm 0.7	0.9 \pm 0.9	2.7 \pm 2.1	1.5 \pm 0.6	0.6 \pm 1.1	1.9 \pm 4.0	0.8 \pm 0.8
FS > 15cm	0.5 \pm 0.0	1.8 \pm 1.1	1.0 \pm 1.1	0.5 \pm 0.6	1.5 \pm 1.0	1.8 \pm 1.9	0.8 \pm 0.7	5.1 \pm 4.9	1.7 \pm 1.2	0.3 \pm 0.5	0.5 \pm 0.5	1.0 \pm 1.2

(c) In-plane Profiles	6 MV			10 MV			18MV			6FFF		
	In-field (%)	Penu mbra (%)	Out-of-field (%)	In-field (%)	Penu mbra (%)	Out-of-field (%)	In-field (%)	Penu mbra (%)	Out-of-field (%)	In-field (%)	Penu mbra (%)	Out-of-field (%)
FS ≤ 5cm	0.6± 0.5	2.0± 0.5	0.4± 0.3	0.5± 0.5	1.3± 0.8	0.5± 0.3	0.8± 0.8	1.5± 0.8	0.6± 0.6	2.0± 1.1	4.9± 0.9	1.6± 0.7
5cm < FS ≤ 15cm	0.5± 0.6	1.8± 1.4	0.8± 0.8	0.6± 0.8	1.4± 0.7	1.0± 0.5	0.8± 0.8	2.6± 2.5	1.4± 0.5	0.6± 0.9	1.5± 3.8	0.9± 1.0
FS > 15cm	0.5± 0.6	2.3± 1.5	1.5± 1.7	0.6± 0.7	1.6± 1.1	1.3± 1.3	0.8± 0.5	4.2± 3.1	1.8± 1.1	0.3± 0.5	0.6± 0.6	1.0± 1.1

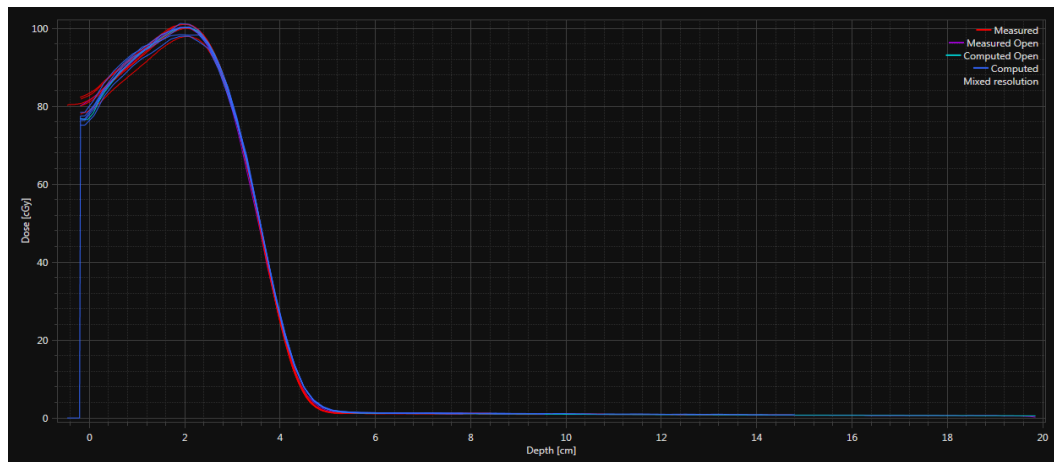
Tolerances for the build-up region = 10%, the fall-off region = 2%, the in-field region = 3%, the penumbra = 10% and the out-of-field region = 3% were employed for evaluations. In terms of PDDs, agreement for all results in fall-off regions was within 0.5% percentage differences, which is far less than the tolerance value. Although build-up quality values appear as large differences, this consequence was produced by the extra data imported before undergoing the modeling process, and descriptions for this phenomenon is shown under the table 2-4 (a). With regard to beam profiles, majority of the results achieved lower than 1% fit quality for in-field and out-of-field regions; some of them contained the difference between 1% to 3%, especially for out-of-field regions with FS wider than 15 cm for all energies and in-field regions with small FS for 6FFF only. Correspondence for all results in the penumbra regions was below 5%, which passed the 10% tolerance without difficulty.

4.1.2 Electrons

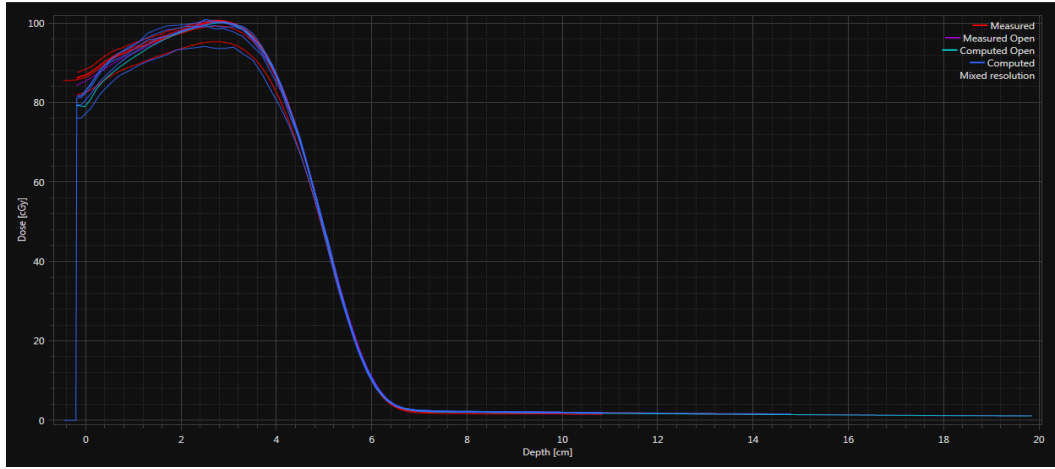
Similar to photons, all matches for PDDs and beam profiles are shown in the figure 4-2 (a-j).



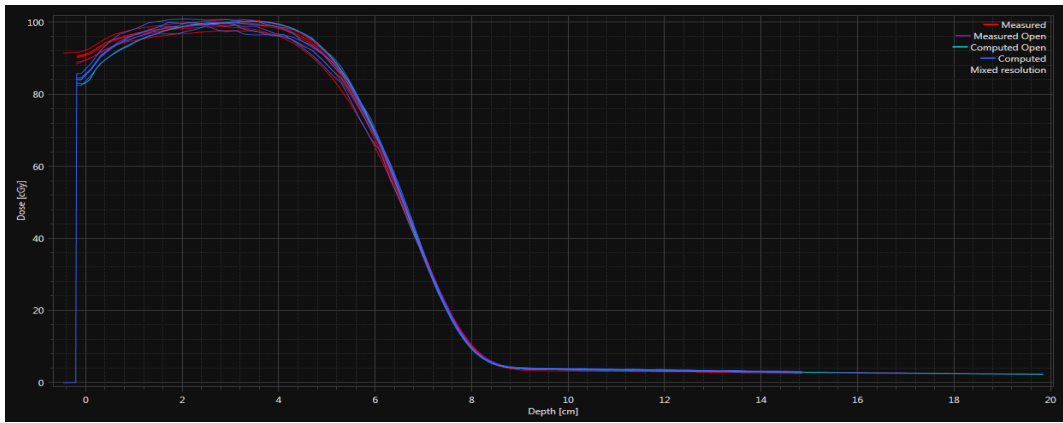
(a)



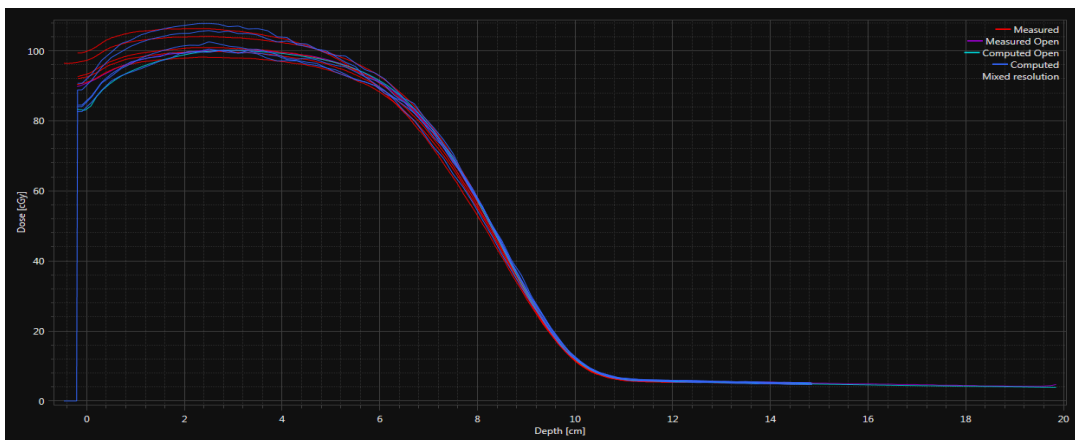
(b)



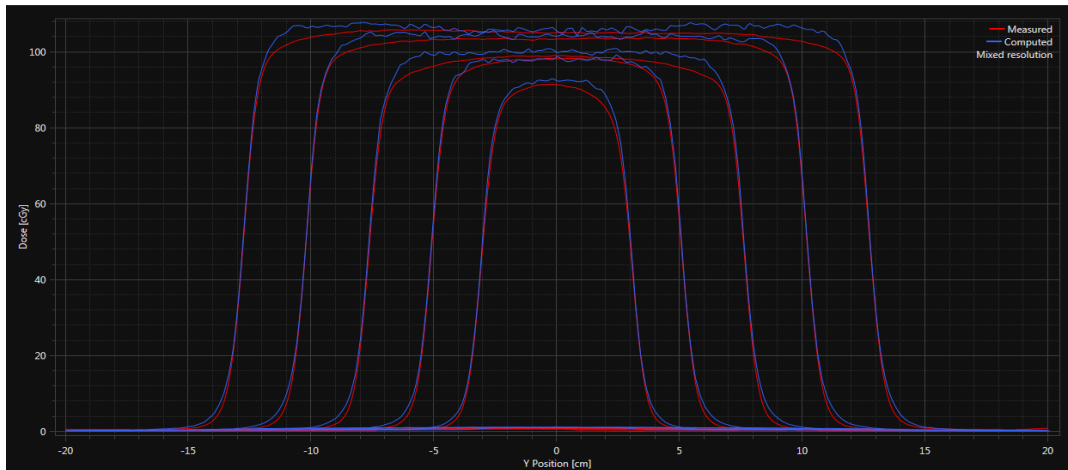
(c)



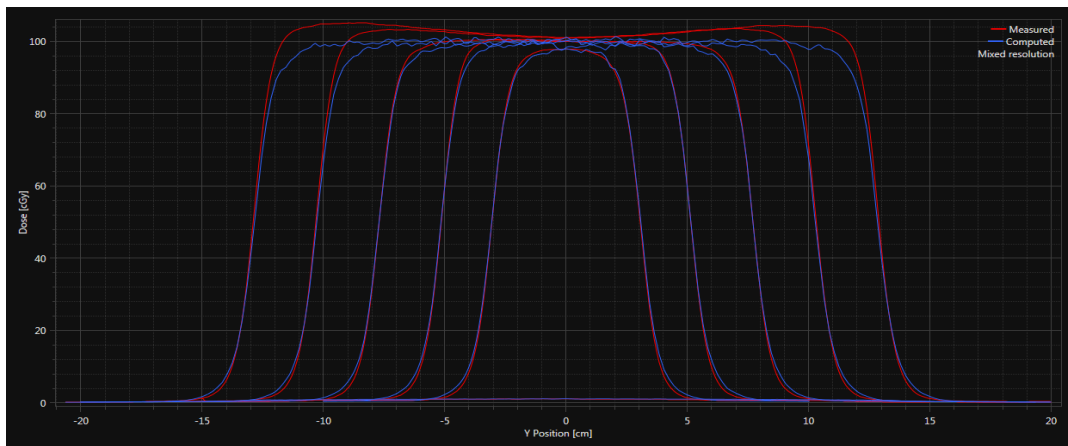
(d)



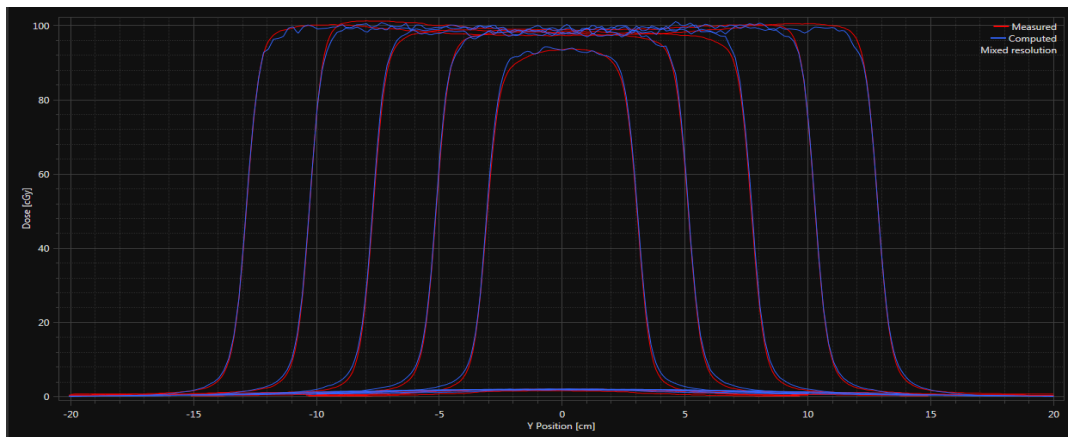
(e)



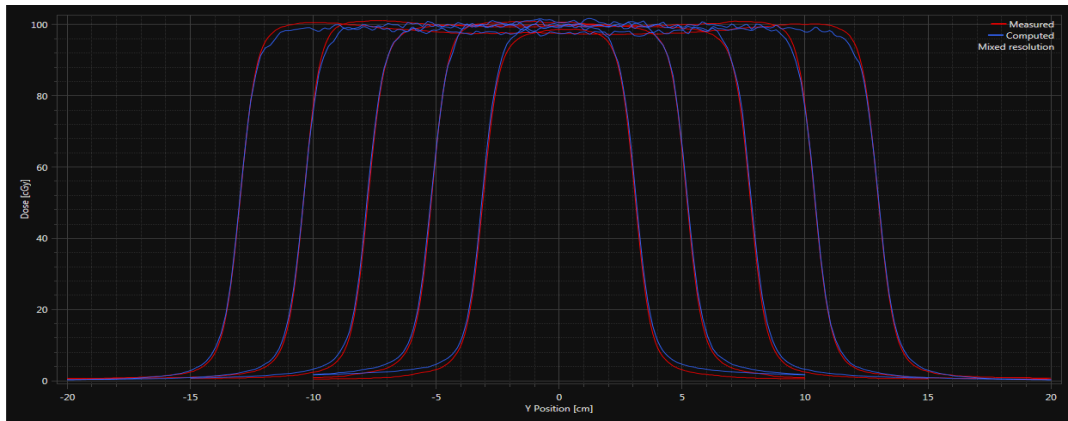
(f)



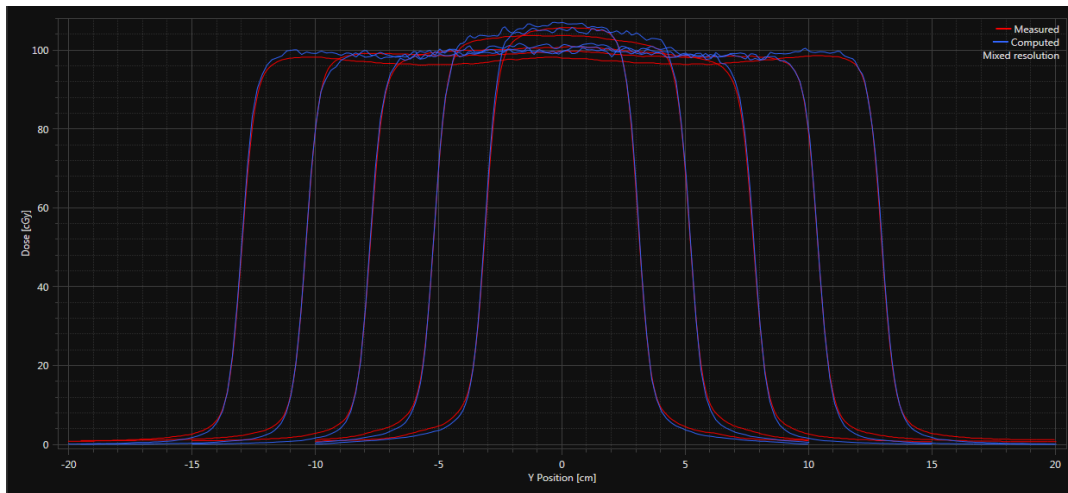
(g)



(h)



(i)



(j)

Figure 4-2: Matches for electron beams' (a) 6 MeV, (b) 9 MeV, (c) 12MeV, (d) 16MeV and (e) 20 MeV PDD curves; continuously followed by in-plane beam profiles for energy of (f) 6 MeV, (g) 9 MeV, (h) 12MeV, (i) 16MeV and (j) 20 MeV, with various applicators respectively.

Evaluating curve qualities by the same method used with photons. Summary of results are displayed in the table 2-5.

Table 4-2: Analysis of fit qualities for (a) PDDs, (b) cross-plane profiles and (c) in-plane profiles.

(a)PDDs	6 MeV	9 MeV	12 MeV	16 MeV	20 MeV
---------	-------	-------	--------	--------	--------

	Build-up (%)	Fall-off (%)								
6 × 6	1.6	0.9	1.5	0.5	2.4	0.8	2.2	0.5	4.1	0.7
10 × 10*	30.9	0.3	27.1	0.8	25.4	0.5	26.4	0.4	29.6	0.7
15 × 15	1.5	0.4	1.5	0.8	1.6	0.2	2.4	0.4	4.0	0.7
20 × 20	1.6	0.6	2.2	1.0	2.3	0.3	2.5	0.5	3.2	0.8
25 × 25	1.7	0.3	1.5	0.5	2.9	0.4	2.6	0.5	3.6	1.3

*Having the same issue mentioned previously with photon's PDDs build-up region. For electron measurements, only 10 by 10 applicator measurements involved unused data above water surface, leading to enormous discrepancies.

(b) Cross-plane Profiles	6 MeV			9 MeV			12 MeV			16 MeV			20 MeV		
	In-field (%)	Pe nu mb ra (%)	Out-of-field (%)	In-field (%)	Pe nu mb ra (%)	Out-of-field (%)	In-field (%)	Pe nu mb ra (%)	Out-of-field (%)	In-field (%)	Pe nu mb ra (%)	Out-of-field (%)	In-field (%)	Pe nu mb ra (%)	Out-of-field (%)
6 × 6	1.9	3.9	0.7	0.8	2.2	0.9	1.3	3.8	0.9	1.6	3.7	1.5	1.5	3.1	0.7
10 × 10	2.1	3.2	1.1	0.7	1.3	1.0	1.6	2.5	0.8	0.8	1.9	1.1	1.7	1.0	1.1
15 × 15	1.7	3.4	1.0	2.3	1.1	0.7	0.9	2.3	0.6	0.8	1.8	0.8	0.9	0.7	0.9
20 × 20	1.4	1.8	0.6	3.3	2.5	0.5	1.1	0.4	0.3	1.3	1.0	0.4	1.0	0.4	0.8
25 × 25	1.6	1.5	0.7	3.7	3.2	0.6	1.0	0.7	0.4	1.2	0.9	0.5	2.0	1.4	0.7

(c) In-plane Profiles	6 MeV			9 MeV			12 MeV			16 MeV			20 MeV		
	In-field (%)	Pe nu mb ra (%)	Out-of-field (%)	In-field (%)	Pe nu mb ra (%)	Out-of-field (%)	In-field (%)	Pe nu mb ra (%)	Out-of-field (%)	In-field (%)	Pe nu mb ra (%)	Out-of-field (%)	In-field (%)	Pe nu mb ra (%)	Out-of-field (%)
6 × 6	2.2	2.5	0.6	0.8	1.1	0.8	1.2	1.8	1.0	1.3	2.6	1.5	1.4	1.4	0.7
10 × 10	1.0	1.9	1.0	1.1	0.8	0.9	0.8	1.3	0.8	0.7	1.6	1.1	1.5	0.7	1.0
15 × 15	2.4	2.7	1.0	1.3	0.8	0.7	1.3	2.0	0.6	0.6	2.3	0.8	0.9	1.6	0.9
20 × 20	1.4	1.3	0.7	3.5	3.0	0.5	0.8	0.7	0.4	1.0	0.9	0.4	0.8	0.6	1.0
25 × 25	1.9	1.7	0.8	3.9	3.8	0.5	0.9	0.5	0.5	1.1	0.7	0.5	1.9	1.5	0.9

Without taking curve quality values of build-up regions for the 10 by 10 applicator size into account for the evaluation, agreement for all results was within 2 %

tolerance in the fall-off region, 10% tolerance in the build-up region, 3% tolerance in the out-of-field region, 10% tolerance in the penumbra and majority of results in the in-field region was lower than 3% tolerance; only percentage differences for 9 MeV in-field with 20 × 20 and 25 × 25 applicator sizes were slightly greater than 3%. Nevertheless, these in-field values will pass the criteria with averages.

4.2 Point dose measurements in homogeneous and inhomogeneous media

Comparisons between measured doses and calculated doses are listed in the table 4-3.

Table 4-3: Results from both actual measurements and RayStation TPS, and percentage errors are included also.

	MLC Retracted Measured Dose (cGy)	MLC Retracted Raystation Dose (cGy)	Error (%)	Error (cGy)
ArcCHECK normal	130.2	131.3	-0.84	-1.10
Lung above	137.3	138.5	-0.87	-1.21
Titanium above	111.4	111.2	0.18	0.20
Muscle above	129.5	132.2	-2.05	-2.71
Lung and muscle above	139.0	141.4	-1.65	-2.33
Titanium and muscle above	105.4	108	-2.44	-2.64
Muscle top titanium bottom	129.5	132.7	-2.42	-3.21
Muscle top lung bottom	129.1	132	-2.17	-2.87
Titanium top lung bottom	109.3	111.1	-1.65	-1.83
Titanium top muscle bottom	110.3	111.2	-0.78	-0.87
Lung top muscle bottom	140.1	138.5	1.18	1.63
Lung top titanium bottom	140.1	139.1	0.74	1.03
Lung top titanium bottom off axis	130.9	130.3	0.47	0.61
Titanium top lung bottom off axis	131.6	131.9	-0.21	-0.28
Titanium top lung bottom off axis (X1 jaw closed)	134.1	136.2	-1.54	-2.10
Titanium top lung bottom off axis (X2 jaw closed)	18.4	14.5	27.23	3.95

The recommended point dose tolerance in inhomogeneous medium for central axis point dose measurement is 3%. All results were within this tolerance except for the last measurement, and this consequence was acceptable due to the data was collected when the detector was not in the radiation area.

4.3 Point dose measurements in a water tank

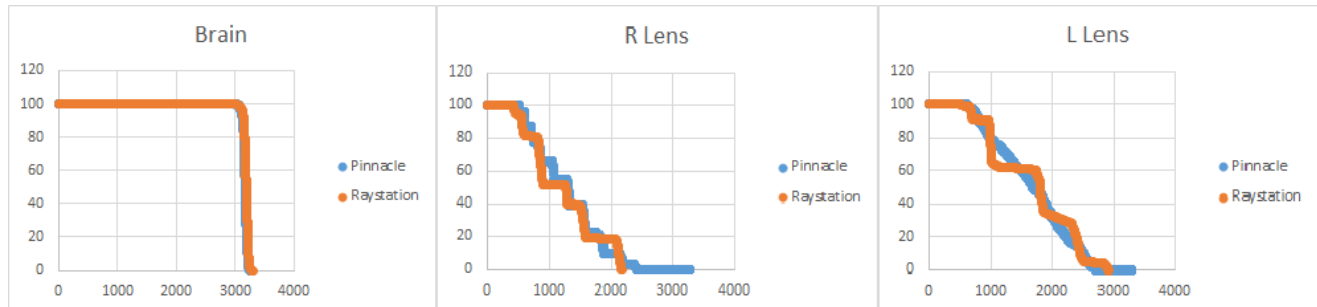
Results of comparison are shown in Appendix B. Percentage differences of central axis point dose measurements are all within 2% for square fields and rectangular fields, however, large deviations of results for the L-shape field are observed which is attributed to the center of the irregular field being blocked by MLCs, where tiny dose fluctuations cause huge divergences. Moreover, observing the position of measured points in the L-shape irregular field in Figure 2-16, the measured point at the center was placed exactly within the interleaf region. According to RaySearch documents, tongue-and-groove regions are only modeled for MLC leaf edges where the edge is exposed into the MLC opening. For MLC leaf edges that are closed against another MLC leaf, no tongue-and-groove regions are added. This effect also has the ability to enlarge differences between measured and computed doses. The best way to decline errors will be shifting the measured point either downstream or upstream for about 2 mm to move the point out of the tongue-and-groove region and repeating measurements.

In terms of off-axis results for both rectangular fields and L-shape fields, massive differences were found. Due to the reason that transmissions for y jaws were designed to be zero during modeling in RayStation, it can be noticed that larger errors happened

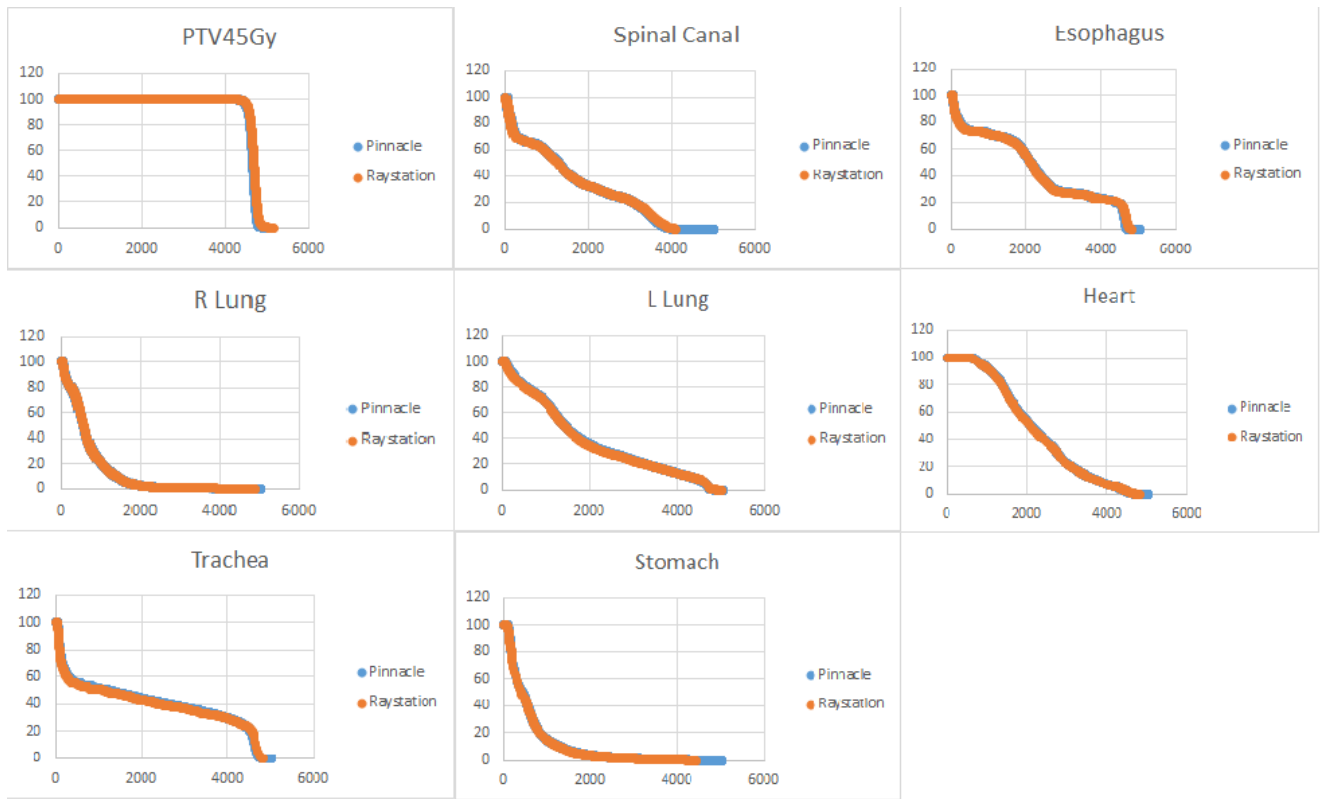
when measured points were blocked by y jaws. Another reasonable explanation for this outcome would be that the majority of off-axis measurements were completed either at the edge of the field (the penumbra region) or not in the field. In accordance with beam modeling results, the penumbra region contained higher percentage differences, and dose drops off sharply within the penumbra region, so less accuracy of the position of the detector will produce larger errors. Furthermore, doses obtained from the blocked region were around 3 cGy, which was very small when comparing with doses measured along the CAX (approximately 200 cGy in average), and tiny discrepancies will result in huge percentage errors.

4.4 Treatment plans comparison for validation

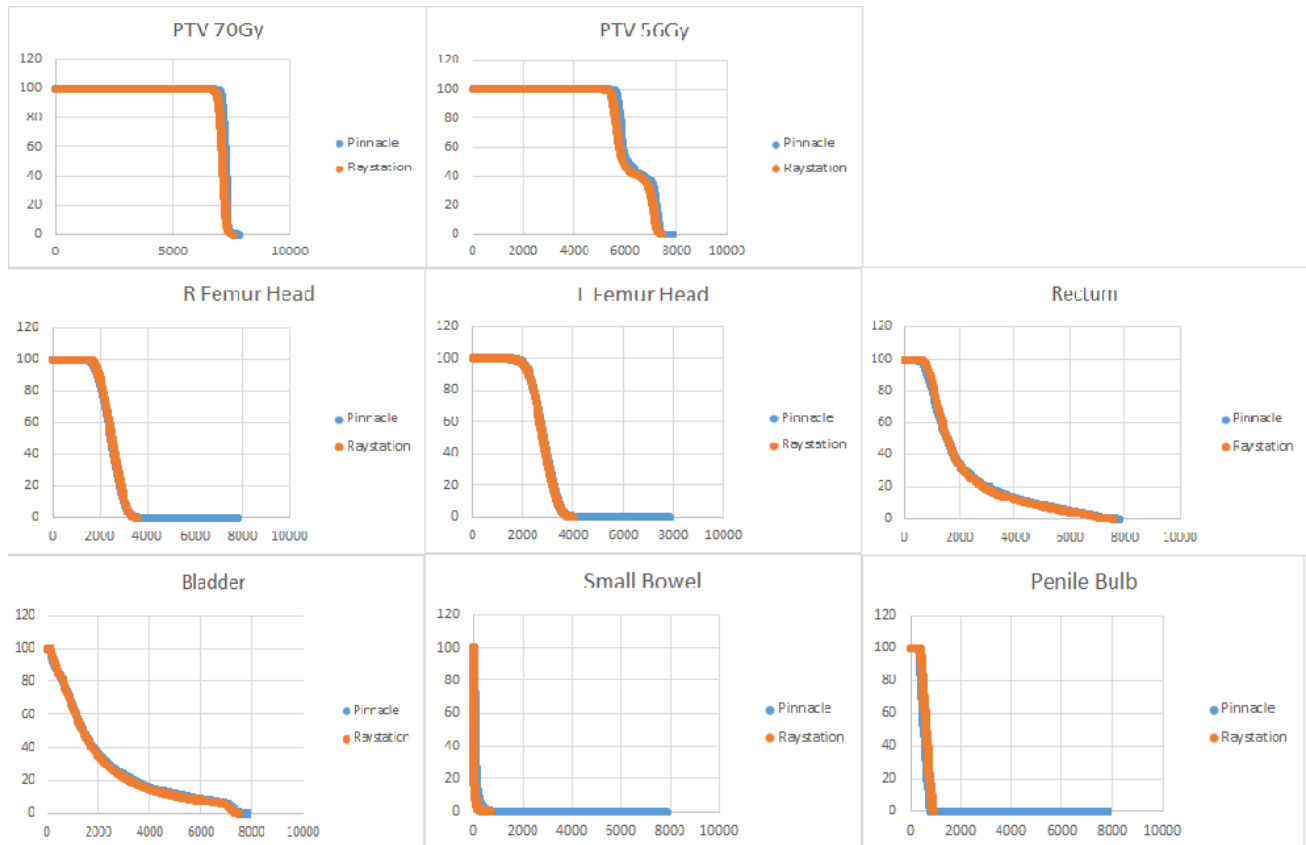
Comparison of DVHs between Raystation and Pinnacle TPSs for all types of treatment plans mentioned above are shown in figure 4-3.



(a)



(b)



(c)

Figure 4-3: DVHs comparison for (a) 3D whole brain plan, (b) IMRT mediastinum and lung cancer plan as well as (c) VMAT prostate cancer plan. The x axis represents doses in cGy, and the y axis represents volume in percentage for all DVHs.

For whole brain plans, DVHs in the PTV region (the brain contour) were identical to each other, however, DVHs in the right and left lens were not matching well but followed the same pattern due to the reason that these organs both locates near the edge of lateral fields, which is the penumbra region causing dramatic dose changes with a tiny distance.

Investigating either VMAT or IMRT plans, every DVH for PTVs and organs at risk performed by Pinnacle and RayStation is overlapping nearly perfectly with each

other. Despite the fact that doses delivered in the PTV region for the prostate cancer plan were slightly higher in Pinnacle, but the differences were still in the acceptable range.

4.5 Discussions

4.5.1 Beam modeling

For photon PDDs, as shown in results, the actual percentage differences in the build-up region were not presented with redundant measured data imported, and the best way to get rid of this problem is cautiously removing those data manually before importing for modeling, however, good agreement still is achieved if considering the entire PDD curves. From the surface to a depth of approximately 2 mm, the fitting results for both electron and photon PDDs won't match ideally, which is indicated in the RayStation Physics document as well.

When it comes to photon beam profiles, it was realized that most of percentage differences in out-of-field regions were worse than in in-field regions. The possible justification might be the no-tilt kernel approximation in the RayStation dose calculation algorithm [7]. In the collapsed cone dose calculating method used in RayStation, all point-spread kernels are aligned with the central axis, which contradicts the reality that scatterings at the edge of fields are not going to be parallel to the central beam axis.

4.5.2 Dosimetric validation

In previous section, it was presented as possible justification for seeing large percentage differences between measured and modeled beams in point doses that this was mostly for points blocked by MLCs or near the field edge. Nearly all other points measured agree reasonably well and attest to the fact that this new treatment planning

system is appropriate to be implemented in clinical use for treating patients on the TrueBeam model.

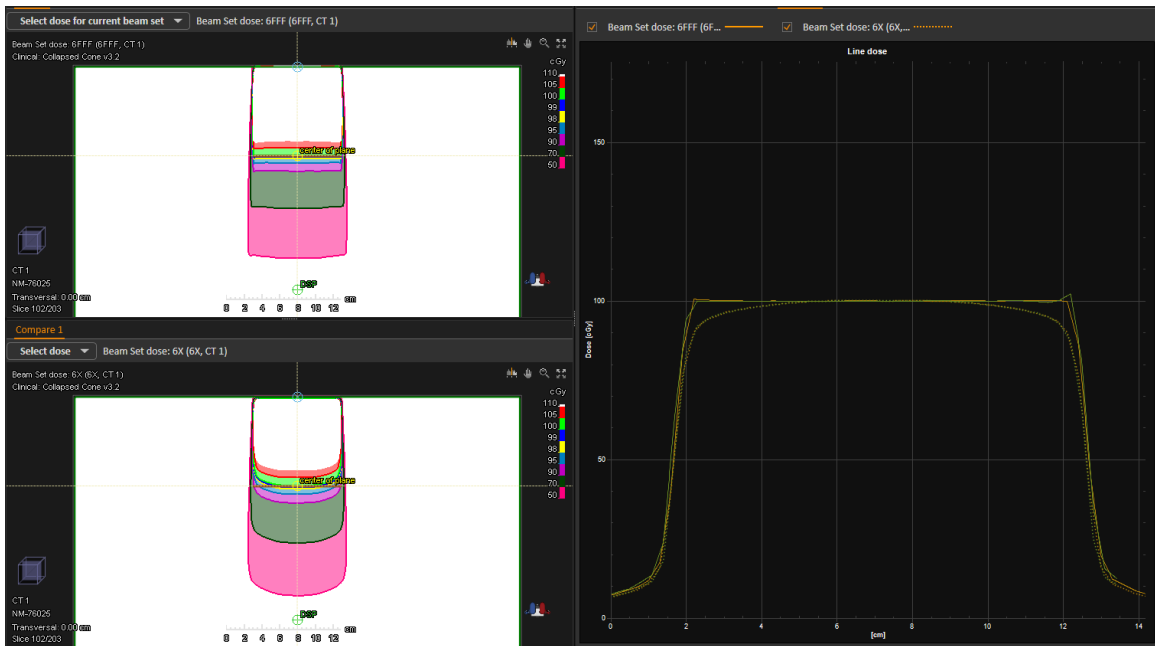
Last but not least, there are further future works that needs to be accomplished. According to AAPM TG-23 report, other than dosimetric tests done in this study, several examinations need to be carried out in the acceptance test, such as the SSD variation and the oblique incidence. Also, beam profiles scanning with wedges presented are required for beam modeling and commissioning as part of the future work.

Chapter 5

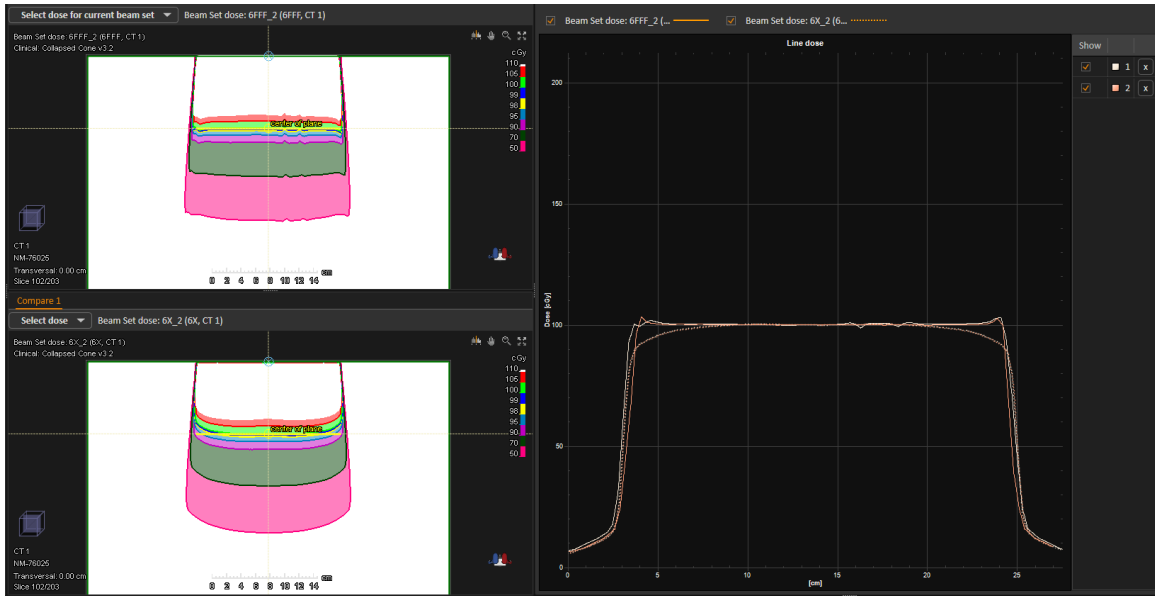
Results and discussions for the feasibility of using FFF Beam to deliver conventional flat beam

5.1 Utilizing flat dose distributions by FFF beams

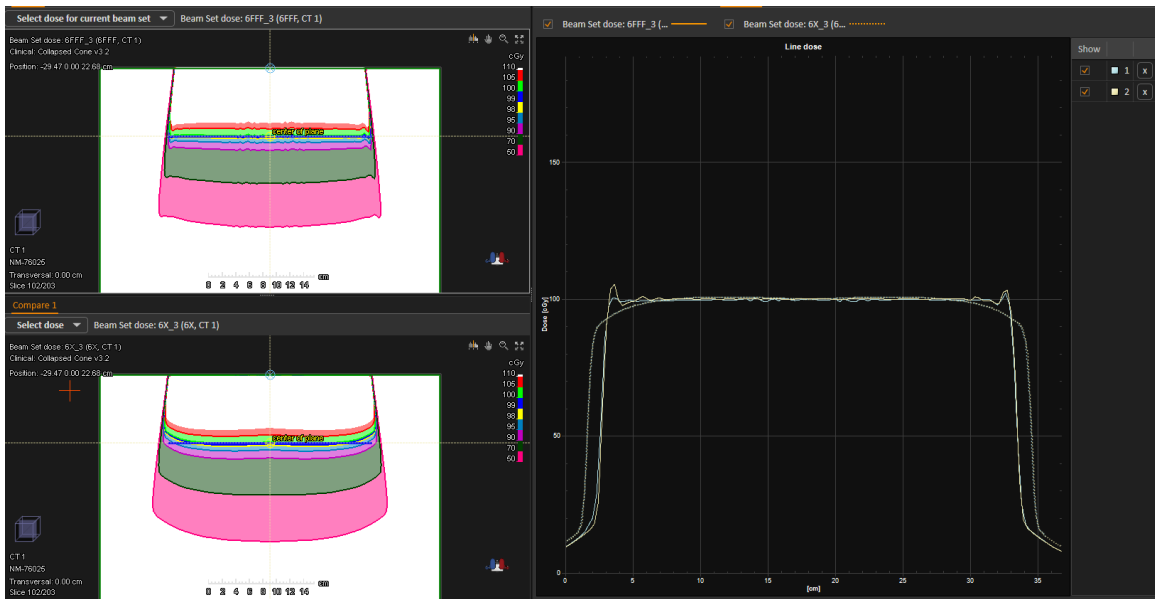
Figure 5-1 shows axial views of dose distributions and line profiles for both FFF beams and flat beams overlaid on top of each other. Each line profile could be exported from the TPS in Excel format data sheet, where it will allow obtaining point dose values along the line. Only data enclosed by the defined-size plane were collected through analyzing processes.



(a) 10×10 FS for the flat beam



(b) 20×20 FS for the flat beam



(c) 30×30 FS for the flat beam

Figure 5-1: Axial views of the dose distribution for the 6 FFF beam (left upper corner) as well as the 6 MV flat beam (left lower corner) in a water cube. On the right side is the cross-line and the in-line dose profile through the CAX at 10 cm depth (the solid line represents 6 FFF and dashed line is 6 MV).

From figure 5-1, it was obviously observed that the FFF beam could achieve an identical uniformity within the region of the square plane as the conventional flat beam or even better. Going a step further to investigate these data, the equation 3 was utilized to quantify the percentage uniformity, and the table 5-1 includes all the results.

Table 5-1: Mean doses, standard deviations and calculated percentage uniformities for respective condition of the flat beam FS as well as the plane size.

6FFF	Average (cGy)	STD (cGy)	Uniformity
Cross-line	99.96	0.18	99.82%
In-line	99.91	0.31	99.69%

6MV	Average (cGy)	STD (cGy)	Uniformity
Cross-line	98.13	2.46	97.49%
In-line	98.1	2.5	97.45%

(a) $10 \times 10 \text{ cm}^2$

6FFF	Average (cGy)	STD (cGy)	Uniformity
Cross-line	100.35	0.52	99.48%
In-line	100.13	0.44	99.56%

6MV	Average (cGy)	STD (cGy)	Uniformity
Cross-line	98.85	1.93	98.05%
In-line	98.77	1.99	97.99%

(b) $20 \times 20 \text{ cm}^2$

6FFF	Average (cGy)	STD (cGy)	Uniformity
Cross-line	99.53	0.75	99.24%
In-line	99.96	0.93	99.07%

6MV	Average (cGy)	STD (cGy)	Uniformity
Cross-line	99.44	1.77	98.22%
In-line	99.43	1.79	98.20%

(c) $30 \times 30 \text{ cm}^2$

Overall, uniformity of the dose across the plane was similar to each other for both beam qualities, additionally, percentage uniformities of the FFF beam were approximately 1% to 2% superior to that of the flat beam.

5.1.1 Discussions

Small distinctness of percentage uniformities between beams with and without the flattening filter within a specific square region demonstrates the feasibility of using a FFF beam to generate the flat dose distribution with the sliding window technique. The reason these field sizes were chosen for this study is that they are the most commonly used range of FS in our clinic; small-field treatment plans are typically implemented on the other accelerator due to the finer resolution of MLCs. Supplementary studies can be explored, for instance, using the same method to compare uniformity with different energies on other LINAC models or different field sizes.

5.2 Clinical treatment plans comparison

New plans completed with 6 FFF beams all achieved the identical percentage coverage of at least one PTV level. Two illustrations of the dose distribution in treatment plans with different patient groups are exhibited in Appendix C. The average maximum dose in plans rose 2.14% for head and neck cancer treatment plans as well as 0.8% for lung and mediastinum cancer treatment plans. Under this condition, all required data noticed before for analysis was collected from DVHs in Pinnacle. Results are shown in the figure 5-2.

Head and neck cancer					
Cord	Average	Mandible	Average	Left submandibular gland	Average
MAX dose difference (Gy)	-2.51	MAX dose difference (Gy)	1.30	MAX dose difference (Gy)	-0.64
mean dose difference (Gy)	-1.63	mean dose difference (Gy)	-0.35	mean dose difference (Gy)	-0.63
V5% (cc)	-0.28	V5% (cc)	-1.63	V5% (cc)	0.00
V10% (cc)	-0.61	V10% (cc)	-0.82	V10% (cc)	0.00
V20% (cc)	-1.33	V20% (cc)	-1.25	V20% (cc)	0.00
V30% (cc)	-2.85	V30% (cc)	-1.31	V30% (cc)	-0.12
Right Parotid	Average	Larynx	Average	Esophagus	Average
MAX dose difference (Gy)	0.28	MAX dose difference (Gy)	-1.01	MAX dose difference (Gy)	-0.04
mean dose difference (Gy)	-1.02	mean dose difference (Gy)	-0.57	mean dose difference (Gy)	-1.27
V5% (cc)	-0.05	V5% (cc)	0.00	V5% (cc)	0.03
V10% (cc)	-0.53	V10% (cc)	0.00	V10% (cc)	-0.01
V20% (cc)	-0.98	V20% (cc)	0.00	V20% (cc)	-0.07
V30% (cc)	-0.61	V30% (cc)	-0.01	V30% (cc)	-0.23
Left Parotid	Average	Right submandibular gland	Average	Oral cavity	Average
MAX dose difference (Gy)	0.87	MAX dose difference (Gy)	-0.54	MAX dose difference (Gy)	0.24
mean dose difference (Gy)	-1.05	mean dose difference (Gy)	-1.52	mean dose difference (Gy)	-0.23
V5% (cc)	-0.13	V5% (cc)	0.00	V5% (cc)	-7.87
V10% (cc)	-0.82	V10% (cc)	0.00	V10% (cc)	-2.21
V20% (cc)	-1.15	V20% (cc)	-0.29	V20% (cc)	-4.02
V30% (cc)	-0.54	V30% (cc)	-0.53	V30% (cc)	-1.88

Lung/mediastinum cancer					
Spinal Canal	Average	Lungs	Average	Trachea	Average
MAX dose difference (Gy)	0.15	MAX dose difference (Gy)	0.16	MAX dose difference (Gy)	0.14
mean dose difference (Gy)	-0.28	mean dose difference (Gy)	-0.24	mean dose difference (Gy)	0.33
V5% (cc)	-0.18	V5% (cc)	-33.98	V5% (cc)	-0.34
V10% (cc)	-0.96	V10% (cc)	-53.46	V10% (cc)	-0.10
V20% (cc)	-0.98	V20% (cc)	-32.88	V20% (cc)	-0.07
V30% (cc)	-0.70	V30% (cc)	-22.02	V30% (cc)	0.01
Esophagus	Average	Heart	Average		
MAX dose difference (Gy)	0.02	MAX dose difference (Gy)	0.85		
mean dose difference (Gy)	-0.58	mean dose difference (Gy)	-0.15		
V5% (cc)	-0.15	V5% (cc)	-3.05		
V10% (cc)	-0.17	V10% (cc)	-8.08		
V20% (cc)	-0.58	V20% (cc)	-10.85		
V30% (cc)	-0.54	V30% (cc)	-11.38		

Figure 5-2: Differences of average maximum doses, mean doses and volumes receiving 5%, 10%, 20% and 30% of the prescription dose between 6 MV and 6 FFF energies for each organ at risk.

Differences were the subtraction between average values from 6 FFF and 6 MV treatment plans, thus the negative sign means doses or volumes were less in the plans with FFF beams presented. In regards to head and neck plans, concurrence for majority of the results was volumes of each adjacent critical structure receiving low doses in FFF beams-based plans were being reduced; others remained the same. This phenomenon occurred significantly for V20% and V30% in the cord and the oral cavity. Moreover, mean doses for critical structures declined also with new plans. However, maximum doses slightly increased in the mandible, both sides of the parotid and the oral cavity since some parts of these organs are in the PTV region. Similar trends with much more significant dose reduction in normal structures were found for lung and mediastinum cancer treatment plans. The only observed exception was in the trachea, which was a part of PTVs for one patient, and some hot spots were included in those areas, causing a higher mean dose.

5.2.1 Discussions

These results point out it is feasible to deliver a flat beam with a FFF beam and produce a treatment plans with more doses sparing organs at risk. Although FFF might generate higher maximum doses in the whole plan, increase of less than 3% of the maximum dose won't result in any sever biological complications. Trading very small escalation of the maximum point dose with preventing critical structures from receiving redundant low dose seems to be worthy.

Chapter 6

Conclusions

A systematic data collection, modeling procedure and dosimetric validation, has been carried out on the RayStation TPS for photon beams. Based on tolerances recommended from published research, majority of outcomes passed the criteria set forth, and others were reviewed and approved by certified medical physicists with reasonable justifications. Wedged fields are required to be measured in the future work for commissioning. Additionally, a method for electron dosimetric tests needs to be designed to complete the final portion of commissioning of electron beams.

With the commissioned RayStation TPS on the TrueBeam LINAC, the FFF beam has been dosimetrically modified to confirm the ability to deliver a flat beam with various FS from 10 cm to 30 cm by the sliding window technique. Uniformity produced by the FFF beam was achieved approximately 1% to 2% superior to that produced by the open-field conventional flat beam.

Advantages with 6 FFF were also discovered after comparing clinical treatment plans (with 6 FFF beams vs. 6 MV flattened beams) in the Pinnacle TPS. With identical coverages of PTVs, lower doses to normal structures have been achieved with FFF beams

in both types of plans, head and neck cancer as well as lung and mediastinum cases. Dose reductions over 10% for heart and more than 50% for lung volumes were observed for the latter treatment sites.

To conclude, while some additional studies are still planned for the future, such as comparison in other beam energies, in different TPSs and discrepancy between plans generated by FFF beams as well as flat beams when measuring dose distributions and point doses with practical dose delivery on the LINAC unit, this research already adequately attested the concept of using FFF photon beam to deliver conventional flat beam. The removal of the flattening filter helps establish much simpler configurations in the LINAC treatment head, which eliminates quality assurances to the filter, accelerating the dose delivery time and lowering expenses on building (from manufacturers' point of view) and purchasing (from clinical consumers' point of view) the machine.

References

1. Bongile, M.; Koki, M.; Rick, S.; Guy, G.; Dayan, L. (2014), 'Modeling and dosimetric performance evaluation of the RayStation treatment planning system', *Journal of Applied Clinical Medical Physics* 15(5), 29-46.
2. Victor, L. (2015) 'The Difference Between a Collapsed Cone Based and a Monte Carlo Based Dose Calculation Algorithm', Master of Science Thesis, RaySearch Laboratories.
3. Cecilia, B.; Miriam, Z.; E. Heath.; Pedro, V. (2012), 'Monte Carlo modeling and simulations of the High Definition (HD120) micro MLC and validation against measurements for a 6 MV beam', *PubMed*.
4. RaySearch Laboratories. RSL-D-RS-5.0-RPHY-EN-1.0 RayStation 5 RayPhysics Manual. Stockholm, Sweden: RSL; 2015.
5. RaySearch Laboratories. RSL-D-RS-5.0-USM-EN-2.0 RayStation 5 User Manual. Stockholm, Sweden: RSL; 2016.
6. RaySearch Laboratories. RSL-D-RS-5.0-BCDS-EN-1.0 Beam Commissioning Data Specification RayStation 5. Stockholm, Sweden; 2015.
7. Daniel, M.; Peter, B.; John, C.; Bruce, C.; Geoffrey, I.; Douglas, J.; Shirley, J.; Dennis, L.; Radhe, M.; Jan van de, G. (1995), 'Task Group #23: Radiation Treatment Planning Dosimetry Verification', AAPM Report NO.55
8. RaySearch Laboratories. RSL-D-RS-5.0-REF-EN-2.0 RayStation 5 Reference Manual. Stockholm, Sweden: RSL; 2016.

Appendix A

Summary of adjustable beam modeling parameters

Table A-1: Beam modeling parameters for photons (Raystation 5 RayPhysics Manual ^[4])

Parameter	Description
Primary source <ul style="list-style-type: none">▪ x width▪ y width	The width parameters specify the elliptical STD of the Gaussian source intensity distribution at the source position.
Flattening filter source <ul style="list-style-type: none">▪ Effective distance to source▪ Weight▪ Width	The width parameter specifies the radial STD of the Gaussian source intensity distribution at the source position.
Electron contamination <ul style="list-style-type: none">▪ Weight of the source▪ Width of the source▪ Weight of flattening filter electron source▪ Energy spectrum parameters E_0 and C	The width parameter specifies the radial STD of the Gaussian source intensity distribution at the source position. The weight relates electron contribution to the photon contribution. The weight of the flattening filter electron source relates the secondary electron contribution to the total electron contribution. Energy spectrum can be shaped by E_0 and C

<p>MLC</p> <ul style="list-style-type: none"> ▪ Effective distance to source ▪ Transmission ▪ Tongue and groove ▪ Leaf tip width ▪ Collimator calibration coefficients x offset, gain, and curvature. 	<p>Offset was read from the measured curves. Tongue-and-groove, leaf-tip-width and collimator calibration coefficients are defined at the projection onto the isocenter plane.</p>
<p>Y jaws</p> <ul style="list-style-type: none"> ▪ Effective distance to source ▪ Position calibration coefficients y offset, gain and curvature. 	<p>The transmission of the Y jaws is zero for a machine with MLC type set to X. The collimator calibration coefficients are defined at the projection onto the isocenter plane.</p>
<p>X jaws</p> <ul style="list-style-type: none"> ▪ Effective distance to source ▪ Transmission ▪ Collimator calibration coefficients x offset, gain and curvature. 	<p>The collimator calibration coefficients are defined at the projection onto the isocenter plane.</p>
<p>Off axis</p> <ul style="list-style-type: none"> ▪ Beam profile correction ▪ Off axis softening 	<p>The beam profile correction is applied as an extra radially dependent scaling of the primary fluence. The off axis softening is given as the water equivalent geometric thickness, and the thickness is zero in the center and otherwise negative. The radius is defined in the projection onto the isocenter plane.</p>
<p>Photon energy spectrum fluence</p>	<p>The energy spectrum of photons at the central axis at the isocenter plane.</p>
<p>Output factor corrections</p>	<p>Normalize the beam monitor measurement to take field size variations into account. Found by fitting to measured output factors, is usually close to 1 for all field sizes.</p>

Table A-2: Beam modeling parameters for electrons (Raystation 5 RayPhysics Manual)

For electron energy spectrum

Parameter	Description
B	The constant term in the linear low-energy tail.
K (MeV⁻¹)	The linear coefficient in the low-energy tail.
E₀ (MeV)	The location of the inflection points of the rising slope.
Delta E (MeV)	The displacement between the inflection points of the rising and declining slopes.
SlopeLow (MeV)	The steepness of the low-energy side of the peak.
Slopehigh (MeV)	The steepness of the high-energy side of the peak.
E_{cut}(MeV)	The low energy cutoff below which the energy spectrum is zero.

For contamination photons

Parameter	Description
Width	The width of the Gaussian distribution which describes the fluence of the contamination photon.
Photon dose normalization	A multiplicative factor scaling the photon contamination dose. This factor is used for all applicator curves for the current beam energy.
Cutout transmission	The amount of the photon fluence that passes through the cutout. This value can be obtained from material specifications or supplementary measurements.
Applicator transmission	How much of contamination photon fluence passes the applicator, but only used for the case where there is no cutout.

Relative photon weight	The amount of contamination photon fluence to be used when fitting the electron spectrum parameters to the open water depth dose curve.
At depth	The depth at which the relative photon weight is specified.

For Source phase space

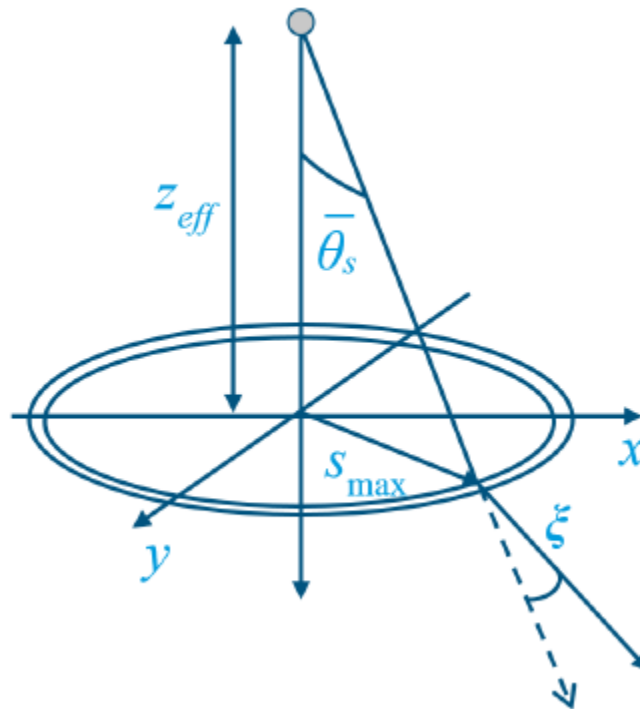


Figure A-1: Electron source phase space parameters

Parameter	Description
Fluence distribution width	The width of Gaussian radial distribution of electrons at the source phase space plane (the secondary scattering foil).
Fluence cut-off radius (S_{max})	The extent of the circular disc from where the electrons appear to come.
Distance to virtual source (z_{eff})	The distance between the source phase space plane and the virtual source point. This factor controls the average polar scattering angle of the generated electrons.
Angular spread on axis (mean θ_s)	The width of the Gaussian distribution of the polar angle spreading over on axis.

Angular spread at cut-off radius	The width of the polar angle smearing at the cut-off radius. Typically, this factor is smaller than the angular spread on axis.
Angular spread curvature	For curvature equals to 1, the angular spread will be a linear function. For curvature less than 1, the angular spread curve will approach the angular spread at cut-off radius faster. For curvature larger than 1, the effect will be opposite.

Appendix B

Results of point dose measurements in the water tank for commissioning

Table B-1: Measured point doses in the water tank for (a) CAX measurements at different depths for every field type, (b) off-axis measurements at 10 cm depth for rectangular fields, and (c) in-field, out-of-field, and edge-of-field measurements at 10 cm depth for irregular fields.

(a)

Energy	Field Type	X-Jaws (cm)	Y-Jaws (cm)	Depth = d_m (cGy)	Depth = 5 cm (cGy)	Depth = 10 cm (cGy)
6FFF	Square	10	10	203.14	171.05	127.95
6FFF	Rectangular	5	20	200.91	167.23	123.29
6FFF	Irregular (L-Shape)	12	12	8.10	12.44	14.83
6MV	Square	10	10	201.42	173.17	133.33
6MV	Rectangular	5	20	199.19	169.35	128.92
6MV	Irregular (L-Shape)	12	12	9.58	12.94	15.52
10MV	Square	10	10	202.69	184.76	148.14
10MV	Rectangular	5	20	199.89	181.60	144.38
10MV	Irregular (L-Shape)	12	12	10.43	11.32	13.29
18MV	Square	10	10	201.59	193.39	158.95
18MV	Rectangular	5	20	198.25	190.39	155.50
18MV	Irregular (L-Shape)	12	12	12.15	10.88	11.72

(b)

Energy	Field Type	X +7.75* cm (cGy)	X +2.75 cm (cGy)	Y +11** cm (cGy)	Y +16 cm (cGy)
6FFF	Rectangular	4.40	77.88	18.83	2.33
6MV	Rectangular	4.13	86.64	25.92	2.54

10MV	Rectangular	3.00	101.46	32.66	1.96
18MV	Rectangular	2.37	97.95	37.86	1.58

(c)

Energy	Field Type	X -2.2 cm, Y -2.2 cm (cGy)	Y +2.2 cm, X +2.2 cm (cGy)	X -2.2 cm, Y +2.2 cm (cGy)	X -4.4 cm, Y -2.2 cm (cGy)	Y +4.4 cm, X +2.2 cm (cGy)	X -4.4 cm, Y +4.4 cm (cGy)
6FFF	Irregular (L-Shape)	76.12	95.04	114.55	114.75	115.06	112.80
6MV	Irregular (L-Shape)	85.96	103.01	126.43	133.53	133.70	137.09
10MV	Irregular (L-Shape)	104.40	110.62	138.79	148.74	150.58	152.33
18MV	Irregular (L-Shape)	101.40	118.51	145.35	161.75	162.26	164.80

*All measured points were shifted from the center of the plane at 10 cm depth. The positive sign means the measured point was set to shift to the left side from the center in the patient coordinate along the x direction, and the negative sign represents that point was set to the right side from the center along the x direction.

**All measured points were shifted from the center of the plane at 10 cm depth. The positive sign means the measured point was set to shift to the superior side from the center in the patient coordinate along the y direction, and the negative sign represents that point was set to the inferior side from the center along the x direction.

Table B-2: Computed point doses in the RayStation TPS for (a) CAX measurements at different depths for every field type, (b) off-axis measurements at 10 cm depth for rectangular fields, and (c) in-field, out-of-field, and edge-of-field measurements at 10 cm depth for irregular fields.

(a)

Energy	Field Type	X-Jaws (cm)	Y-Jaws (cm)	Depth = d_m (cGy)	Depth = 5 cm (cGy)	Depth = 10 cm (cGy)
6FFF	Square	10	10	199.90	168.30	126.30
6FFF	Rectangular	5	20	197.10	164.10	121.50
6FFF	Irregular (L-Shape)	12	12	8.20	11.10	12.80
6MV	Square	10	10	199.50	172.40	133.40
6MV	Rectangular	5	20	195.90	167.60	128.10
6MV	Irregular (L-Shape)	12	12	9.30	11.80	14.00
10MV	Square	10	10	200.00	183.50	147.80
10MV	Rectangular	5	20	197.20	180.30	143.60

10MV	Irregular (L-Shape)	12	12	13.80	13.90	15.00
18MV	Square	10	10	201.20	192.40	159.50
18MV	Rectangular	5	20	197.50	188.50	155.00
18MV	Irregular (L-Shape)	12	12	9.90	8.80	9.90

(b)

Energy	Field Type	X +7.75 cm (cGy)	X +2.75 cm (cGy)	Y +11 cm (cGy)	Y +16 cm (cGy)
6FFF	Rectangular	3.20	58.70	40.40	1.50
6MV	Rectangular	3.00	63.50	54.40	1.60
10MV	Rectangular	2.80	71.20	59.40	2.50
18MV	Rectangular	1.50	75.50	65.80	0.80

(c)

Energy	Field Type	X -2.2 cm, Y -2.2 cm (cGy)	Y +2.2 cm, X +2.2 cm (cGy)	X -2.2 cm, Y +2.2 cm (cGy)	X -4.4 cm, Y -2.2 cm (cGy)	Y +4.4 cm, X +2.2 cm (cGy)	X -4.4 cm, Y +4.4 cm (cGy)
6FFF	Irregular (L-Shape)	69.00	62.50	97.00	114.20	114.20	112.40
6MV	Irregular (L-Shape)	81.70	68.90	110.60	133.30	133.30	136.40
10MV	Irregular (L-Shape)	85.90	76.80	119.90	146.30	146.60	150.20
18MV	Irregular (L-Shape)	91.20	82.30	128.90	163.80	163.80	166.00

Table B-3: Percentage point dose differences of (a) CAX measurements at different depths for every field type, (b) off-axis measurements at 10 cm depth for rectangular fields, and (c) in-field, out-of-field, and edge-of-field measurements at 10 cm depth for irregular fields between measured data and computed data in RayStation in the water tank.

(a)

Energy	Field Type	X-Jaws (cm)	Y-Jaws (cm)	Depth = d_m (%)	Depth = 5 cm (%)	Depth = 10 cm (%)
6FFF	Square	10	10	1.62	1.63	1.31
6FFF	Rectangular	5	20	1.93	1.91	1.47
6FFF	Irregular (L-Shape)	14.33	15.26	-1.27	12.04	15.85

6MV	Square	10	10	0.96	0.45	-0.05
6MV	Rectangular	5	20	1.68	1.05	0.64
6MV	Irregular (L-Shape)	14.33	15.26	3.01	9.66	10.89
10MV	Square	10	10	1.35	0.69	0.23
10MV	Rectangular	5	20	1.37	0.72	0.55
10MV	Irregular (L-Shape)	14.33	15.26	-24.45	-18.57	-11.42
18MV	Square	10	10	0.19	0.51	-0.35
18MV	Rectangular	5	20	0.38	1.00	0.32
18MV	Irregular (L-Shape)	14.33	15.26	22.71	23.62	18.39

(b)

Energy	Field Type	X +7.75* cm (%)	X +2.75 cm (%)	Y +11** cm (%)	Y +16 cm (%)
6FFF	Rectangular	37.41	32.67	53.39	55.15
6MV	Rectangular	37.52	36.44	52.36	58.88
10MV	Rectangular	7.15	42.50	45.02	21.62
18MV	Rectangular	57.98	29.74	42.46	97.23

(c)

Energy	Field Type	X -2.2 cm, Y -2.2 cm (%)	Y +2.2 cm, X +2.2 cm (%)	X -2.2 cm, Y +2.2 cm (%)	X -4.4 cm, Y -2.2 cm (%)	Y +4.4 cm, X +2.2 cm (%)	X -4.4 cm, Y +4.4 cm (%)
6FFF	Irregular (L-Shape)	10.32	52.06	18.09	0.48	0.75	0.35
6MV	Irregular (L-Shape)	5.22	49.51	14.31	0.17	0.30	0.50
10MV	Irregular (L-Shape)	21.54	44.04	15.75	1.67	2.71	1.42
18MV	Irregular (L-Shape)	11.19	44.00	12.76	-1.25	-0.94	-0.72

Appendix C

Clinical treatment plans comparison



Figure C-1: Example of the sagittal-view dose distribution in a head and neck cancer treatment plans. (Left side was planning with flat beams and right side was done with FFF beams).

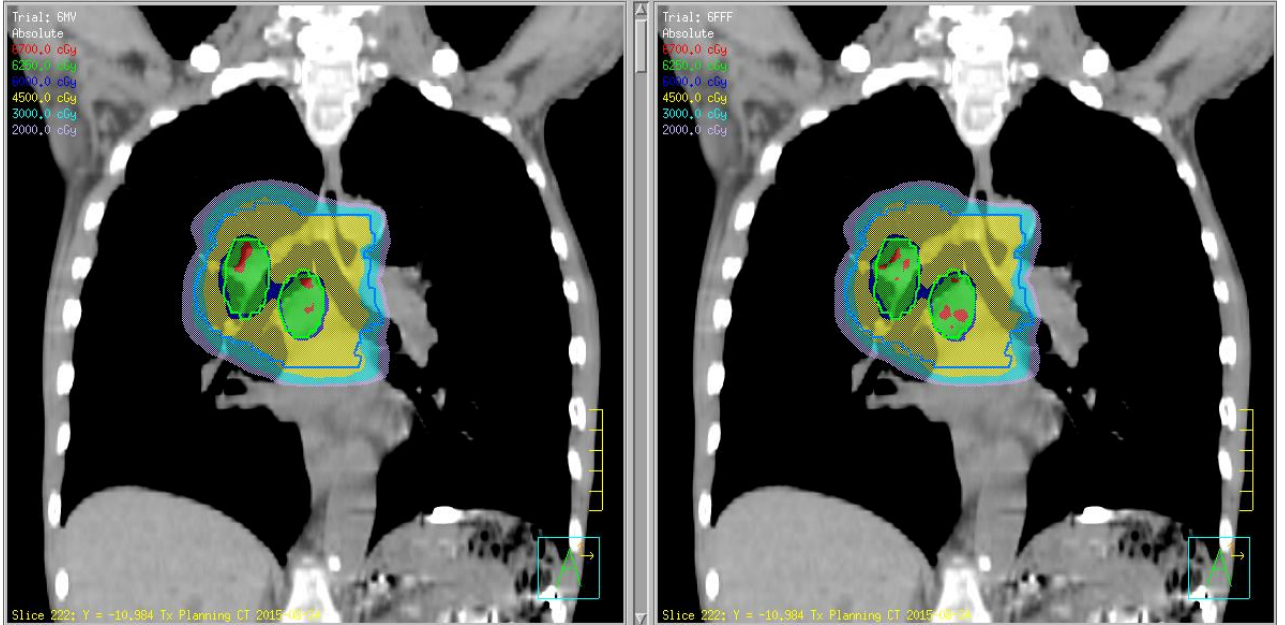


Figure C-2: Example of the coronal-view dose distribution in a lung and mediastinum cancer treatment plans. (Left side was planning with flat beams and right side was done with FFF beams).